Zircon inheritance, sources of Devonian granitic magmas and crustal structure in central Victoria

J. D. Clemens, G. Stevens and L. M. Coetzer

Department of Earth Sciences, University of Stellenbosch, South Africa

ORCID

J. D. Clemens https://orcid.org/0000-0002-8748-1569

G. Stevens https://orcid.org/0000-0003-1593-9419

CONTACT J. D. Clemens email jclemens@sun.ac.za mail Department of Earth Sciences, University of Stellenbosch, Private Bag X1, Matieland 7602, South Africa

SUPPLEMENTAL DATA

Copies of Supplementary Papers may be obtained from the Geological Society of Australia's website (www.gsa.org.au), the Australian Journal of Earth Sciences website (www.ajes.com.au) or from the National Library of Australia's Pandora archive (https://pandora.nla.gov.au/tep/150555).

Supplemental data

Paper 1. Sample preparation and analytical details.

Paper 2. Analytical data for samples and standards. (Excel spreadsheet)

Paper 3. Descriptions of zircon populations in new samples.

Paper 4. A selection of Wetherill concordia plots for analysed granitic, metamorphic and sedimentary rocks.

Paper 5. Igneous and metamorphic age spectra of inherited zircon in newly analysed samples.

Supplementary Paper 1

Sample preparation and analytical details

Whole-rock major-oxide and trace-element analyses of new samples (VH2, AD1, MB1 and S12)

Samples were crushed with a jaw crusher and milled to a fine powder in a tungsten disc mill prior to the preparation of a fused disc for major- and trace-element analysis. The jaw crusher and mill were cleaned with uncontaminated quartz between samples, to avoid cross contamination. Glass disks were prepared for XRF analysis using 10 g of high purity trace-element- and REE-free flux ($LiBO_2$ = 32.83%, $Li_2B_4O_7$ = 66.67%, LiI = 0.50%) mixed with 0.8 g of the rock sample. Whole-rock major-element compositions were determined by XRF spectrometry on a PANalytical Axios Wavelength Dispersive spectrometer. The spectrometer is fitted with an Rh tube and with the following analysing crystals: LIF200, LIF220, LIF420, PE and PX1. The instrument is fitted with a gas-flow proportional counter and a scintillation detector. The gas-flow proportional counter uses a 90% Argon, 10% methane gas mixture. Major elements were analysed on a fused glass disk at 50 kV and 50 mA tube operating conditions. Matrix effects in the samples were corrected for by applying theoretical alpha factors and measured line overlap factors to the raw intensities measured with the SuperQ PANalytical software. Internal standards were basalt BHVO-1 and granodiorite JG-1. For the granodiorite, relative uncertainties (the standard errors for the JG-1, in wt%) are; SiO_2 = 0.69, TiO_2 = 1.120, Al_2O_3 = 0.48, FeO_T = 1.05, MnO = 0.00, MgO = 1.16, CaO = 0.05, Na_2O = 0.18, K_2O = 0.70 and P_2O_5 = 1.92. For the basalt, relative uncertainties (the standard errors for the BHVO-1, in wt%) are; SiO_2 = 0.23, TiO_2 = 2.71, Al_2O_3 = 0.58, FeO_T = 0.32, MnO = 0.00, MgO = 0.47, CaO = 0.35, Na_2O = 4.69, K_2O = 3.70 and P_2O_5 = 0.74. Results are reported normalised to 100 wt% volatile-free, with total Fe expressed as FeO_T.

Whole-rock Sr and Nd isotope analyses of new samples

For each sample, approximately 50 mg of powder was weighed into a Teflon beaker and about 4 mL 4:1 concentrated 2B $HF:HNO_3$ was added. The beaker was then capped and left to digest on a hot plate for at least 2 days. The resulting solution was dried and re-dissolved in 6M 2B HNO_3, twice. After the second drying, the sample was taken up in 1.5 mL of 2M 2B HNO_3. Note that this same solution was used for the Rb, Sr, Sm and Nd analyses (on the quadrupole ICP-MS), as well as the Sr and Nd isotope ratios. After centrifuging, the supernatant was loaded onto a cleaned and pre-conditioned column of 0.2 mL Sr.Spec resin (Eichrom). The column was washed with 2M 2B HNO_3 and the Sr fraction collected in 0.02M 2B HNO_3 (after Míková & Denková, 2007; Pin & Zalduegui, 1997; Pin *et al.*, 1994). Low-Sr, high-Rb samples were subjected to a double pass through the column. Following the final drying, these fractions were re-dissolved in 2 mL of 0.2% HNO_3. Based on the XRF values for Sr concentrations of the original samples, 3 mL of 200 ppb Sr solutions were prepared for analysis using the same 0.2% HNO_3.

Analyses were performed using a NuPlasma HR MC-ICP-MS (Nu Instruments, Wrexham, Wales, UK) in the Department of Geological Sciences at the University of Cape Town. The approximately 200 ppb Sr sample and standard solutions were aspirated into the plasma through a microcyclonic spray chamber. The on-peak background was measured for 120 seconds while aspirating the same 0.2% HNO_3 used to dilute the sample and standard solutions. These background measurements, including any krypton (^{84}Kr and ^{86}Kr) present in the argon gas, were subtracted from the measured signals. Instrumental mass fractionation was corrected using the exponential law and a fractionation factor based on the measured $^{86}Sr/^{88}Sr$ ratio and the accepted value of 0.1194. The ^{87}Rb contribution to the 87 amu signal was calculated and subtracted using this fractionation factor, the exponential law, the measured ^{85}Rb signal and a $^{85}Rb/^{87}Rb$ ratio of 0.3856.

To assess instrument tuning and stability, a 200 ppb Sr solution of the NIST SRM987 international Sr isotope standard was analysed twice, prior to any samples. The external, measured 2σ reproducibility of SRM987 was 0.000019 (n = 3) on an average $^{87}Sr/^{86}Sr$ ratio of 0.710277. All $^{87}Sr/^{86}Sr$ data were normalised to 0.710255, the in-house long-term average, which agrees with published results. The average $^{84}Sr/^{86}Sr$ ratio was 0.05643 ± 0.00012 (n = 4), also in agreement with published values.

Initial $^{87}Sr/^{86}Sr$ ratios and their 2σ uncertainties were calculated from the measured Rb and Sr contents (with 1σ errors) and measured, present-day $^{87}Sr/^{86}Sr$ values (with 2σ measurement variations) using a Monte Carlo simulation routine. Although all isotope ratios were calculated at a reference age of 370 Ma, using the decay constant for ^{87}Rb from Rotenberg *et al.* (2012), overall uncertainties on the calculated initial $^{87}Sr/^{86}Sr$ ratios incorporate a notional age uncertainty of ± 2 Ma.

Nd isotope analyses were carried out using the same multi-collector ICP-MS instrument that was used for the Sr isotope determinations, using the same primary solutions that were used for the Sr isotope work. Nd isotopes were analysed in 1.5 mL of 50 ppb Nd 2% HNO_3 solutions using a Nu Instruments DSN-100 desolvating nebuliser. JNdi-1 was used as bracketing standard, and all Nd isotope data presented are referenced to this standard, using a $^{144}Nd/^{143}Nd$ ratio of 0.512115 (Tanaka *et al.*, 2000). All Nd isotope data were corrected for Sm and Ce interferences and for instrumental mass fractionation, using the exponential law and a $^{146}Nd/^{144}Nd$ value of 0.7219. For further details of the analytical techniques see Will *et al.* (2007). Two-stage, depleted-mantle, Nd model ages were calculated using the methods of Keto and Jakobsen (1987), with present-day depleted mantle values of $^{143}Nd/^{144}Nd = 0.513151$ and $^{147}Nd/^{144}Nd = 0.2136$.

Zircon recovery

The samples were slabbed using a diamond saw, broken into pieces of about 25 mm Å ~12 mm, and then processed in the SELFRAG facility at the University of Pretoria, to fragment rocks without damaging the zircon grains. Zircon crystals were then concentrated using the panner and Franz electromagnetic separator in the Central Analytic Facilities at SU. Zircons crystals were then hand-picked from the concentrate and mounted, in lines, in epoxy-resin moulds that were then polished.

SEM Cathodoluminescence Imaging

The zircon grains were imaged using cathodoluminescence scanning electron microscopy, in the Central Analytical Facilities at SU. The images of the crystals and selected inherited cores were marked with 30 µm rings to indicate the spots to be analysed. Descriptions of the samples and their zircon populations can be found in Supplementary Paper 3.

Zircon U–Pb chronology

All U–Pb data were obtained at the Central Analytical Facilities (SU) by laser ablation-single collector magnetic sector field-inductively coupled plasma-mass spectrometry (LA-SF-ICP-MS). Data collection employed a Thermo Finnigan Element2 mass spectrometer coupled to either a Resonetics S155 193 nm excimer laser ablation system with a Laurin Helix double-volume cell. Instrument operating conditions are summarised in Table A1.1.

Zircon U–Pb isotope data were obtained by single-spot analyses, with a spot diameter of 20 µm and a crater depth of approximately 15 to 20 µm. The methods employed for analysis and data processing are described in detail by Gerdes and Zeh (2006) and Frei and Gerdes (2009) and are summarised in Table A1.1. Data reduction used an in-house Excel spreadsheet. Common Pb correction of the zircon U–Pb isotope ratios were not done. Zircon Th and U concentrations were calculated from measured counts on ^{232}Th and ^{236}U in the unknown and GJ-1 zircon standard, normalised to measured Th and U concentrations of 12.9 and 512 ppm for the GJ-1 chip used at SU. Uncertainties on the tabulated U–Pb isotope data and spot ages are given at the 2σ level. The calculation of concordia ages and plotting of concordia diagrams were performed using IsoplotR (Vermeesch, 2018). The plots of probability density distributions for the spot ages for each sample were made for spots with concordances between 90 and 110%, using a bin width of 5 Myr, with both instrumental uncertainty and a bandwidth of 30 Myr applied.

Matrix-matched dating used the GJ-1 zircon reference material (TIMS $^{207}Pb–^{206}Pb$ age = 608.53 ± 0.37 Ma; Jackson *et al.*, 2004) as the primary calibrant. For quality control, the Plešovice (TIMS $^{206}Pb–^{238}U$ age = 337.13 ± 0.37 Ma; Sláma *et al.*, 2008) zircon reference material was also analysed, yielding a concordia age of 337 ± 3 Ma (2012, 2σ, MSWD of concordance and equivalence (C+E) = 0.84). The full analytical dataset for the quality control materials is given in Supplementary Paper 2.

Table A1.1 LA-SF-ICP-MS, U–Th–Pb dating methods.

Laboratory & Sample Preparation	
Laboratory name	Central Analytical Facilities, Stellenbosch University
Sample type / mineral	zircon grain mount
Sample preparation	SELFRAG (U. Pretoria) + conventional mineral separation, 2.5 cm resin mount, 1 µm polish to finish
Imaging	CL, LEO 1430 VP, 10 nA, 15 mm working distance
Laser ablation system	
Make, Model and type	Resolution SE 193 nm Ar F ATL Excimer laser
Ablation cell and volume	Laurin Technic S155 dual-volume large format cell
Laser wavelength	193 nm
Pulse width	5 ns
Fluence	1.9 J/cm$_2$
Repetition rate	9 Hz
Spot size	20 µm
Sampling mode / pattern	20 µm single spot analyses
Cell carrier gas	100% He, Ar and N$_2$ make-up gases combined using injectors into sampling funnel
Pre-ablation laser warm-up (background collection)	3 cleaning shots followed by 20 s background collection
Ablation duration	15 s
Wash-out delay	15 s
Cell carrier gas flows	400 mL/min He
ICP-MS Instrument	
Make, Model and type	Thermo Finnigan Element2 single collector HR-SF-ICP-MS
Sample introduction	via 4mm ID Nylon tubing
RF power	1350 W
Make-up gas flow	910 mL/min Ar and 4 mL/min N$_2$
Detection system	single-collector secondary electron multiplier
Masses measured	202, 204, 206, 207, 208, 232, 238
Integration time per peak	3–15 ms
Total integration time per reading	0.9 s (represents the time resolution of the data)
Sensitivity	30000 cps/ppm Pb
Dead time	6 ns
Data Processing	
Gas blank	10 seconds on-peak
Calibration strategy	GJ-1 zircon used as primary reference material, Plešovice zircon used as secondary reference material (quality control)
Reference Material info	GJ-1 (609 Ma; Jackson *et al.*, 2004); Plešovice (337 Ma; Sláma *et al.*, 2008)
Data processing package used / Correction for LIEF	Iolite software for data normalisation, uncertainty propagation and age calculation. LIEF correction assumes reference material and samples behave identically.
Mass discrimination	Standard-sample bracketing with ^{207}Pb/^{206}Pb and ^{206}Pb/^{238}U normalised to zircon reference material GJ-1.
Common-Pb correction, composition and uncertainty	not applicable
Uncertainty level and propagation	ages quoted at 2σ absolute, propagation by quadratic addition
Quality control / Validation	Plešovice: Concordia age = 338 ± 2 Ma (2σ, MSWD (C+E) = 0.81)
Other information	For detailed method description see Frei and Gerdes (2009)

References

Frei, D., & Gerdes, A. (2009). Precise and accurate in situ U–Pb dating of zircon with high sample throughput by automated LA-SF-ICPMS. *Chemical Geology, 261*(3–4), 261–270. https://doi.org/0.1016/j.chemgeo.2008.07.025

Gerdes, A., & Zeh, A. (2006). Combined U–Pb and Hf isotope LA-(MC)-ICP-MS analyses of detrital zircons: comparison with SHRIMP and new constraints for the provenance and age of an Armorican metasediment in Central Germany. *Earth and Planetary Science Letters, 249*(1–2), 47–61. https://doi.org/10.1016/j.epsl.2006.06.039

Jackson, S., Pearson, N. J., Griffin, W. L., & Belousova, E. A. (2004). The application of laser ablation-inductively coupled plasma-mass spectrometry to in situ U–Pb zircon geochronology. *Chemical Geology, 211*(1–2), 47–69. https://doi.org/10.1016/j.chemgeo.2004.06.017

Keto, L. S., & Jacobsen, S. B. (1987). Nd and Sr isotopic variations of Early Paleozoic oceans. *Earth and Planetary Science Letters, 84*(1), 27–41. https://doi.org/10.1016/0012-821X(87)90173-7

Míková, J., & Denková, P. (2007). Modified chromatographic separation scheme for Sr and Nd isotope analysis in geological silicate samples. *Journal of Geosciences, 52*(3–4), 221–226. https://doi.org/10.3190/jgeosci.015

Pin, C., Briot, D., Bassin, C., & Poitrasson, F. (1994). Concomitant separation of strontium and samarium neodymium for isotopic analysis in silicate samples, based on specific extraction chromatography. *Analytica Chimica Acta, 298*(2), 209–217. https://doi.org/10.1016/0003-2670(94)00274-6

Pin, C., & Zalduegui, J. F. S. (1997). Sequential separation of light rare-earth elements, thorium and uranium by miniaturized extraction chromatography: Application to isotopic analyses of silicate rocks. *Analytica Chimica Acta, 339*(1–2), 79–89. https://doi.org/10.1016/S0003-2670(96)00499-0

Rotenberg, E., Davis, D. W., Amelin, Y., Ghosh, S., & Bergquist, B. A. (2012). Determination of the decay constant of [87]Rb by laboratory accumulation of [87]Sr. *Geochimica et Cosmochimica Acta, 85*, 41–57. https://doi.org/10.1016/j.gca.2012.01.016

Sláma, J., Košler, J., Condon, D. J., Crowley, J. L., Gerdes, A., Hanchar, J. M., Horstwood, M. S. A., Morris, G. A., Nasdala, L., Norberg, N., Schaltegger, U., Schoene, B., Tubrett, M. N., & Whitehouse, M. J. (2008). Plešovice zircon – a new natural reference material for U–Pb and Hf isotopic microanalysis. *Chemical Geology, 149*(1–2). https://doi.org/10.1016/j.chemgeo.2007.11.005

Stacey, J. S., & Kramers, J. D. (1975). Approximation of terrestrial lead isotope evolution by a 2-stage model. *Earth and Planetary Science Letters, 26*(2), 207–221. https://doi.org/10.1016/0012-821X

van Achterbergh, E., Ryan, C. G., Jackson, S. E., & Griffin, W. (2001). Data reduction software for LAICP-MS. In P. Sylvester (Ed.), *Laser ablation-ICPMS in the Earth Sciences* (Vol. 29, pp. 239–243): Mineralogical Association of Canada.

Vermeesch, P. (2018). IsoplotR: a free and open toolbox for geochronology. *Geoscience Frontiers, 9*(5), 1479–1493. https://doi.org/10.1016/j.gsf.2018.04.001

Will, T. M., Frimmel, H. E., Zeh, A., Le Roux, P., & Schmädicke, E. (2010). Geochemical and isotopic constraints on the tectonic and crustal evolution of the Shackleton Range, East Antarctica, and correlation with other Gondwana crustal segments. *Precambrian Research, 180*(1–2), 85–112. https://doi.org/10.1016/j.precamres.2010.03.005

Supplementary Paper 3

Descriptions of zircon populations in new samples

In the following, all sample locations are given as eastings and northings on the Australian National Grid, UTM projection using the WGS84 ellipsoid. Zircon crystals were liberated from their host rocks using the high-voltage, pulsed-power Selfrag instrument at the Department of Geology in the University of Pretoria. Use of this technology guarantees high degrees of liberation of the crystals without damage due to crushing. Thus, most of the zircon crystals described here are complete and unbroken, doubly-terminated crystals. The one negative aspect of using this technique is that even internally fractured, brittle, metamict crystals commonly remain intact and may be present among the analysed grains. Descriptions of internal structures of the zircon grains refer to features visible in SEM CL (cathodoluminescence) images. After each sample is described, a selection of zircon crystals is shown, with analysis numbers and rings showing the analysed spots; unanalysed crystals are marked 'n. a.'. The $^{206}Pb/^{238}U$ ages are also given for spots, with concordance between 90 and 110% in yellow and discordant in white. The terms Melbourne Zone, Bendigo Zone and Stawell Zone refer to fault-bounded structural zones in the Paleozoic metasedimentary rocks of central Victoria, as recognised through their differing internal ages, structural styles, and sedimentological and metamorphic characteristics (VandenBerg *et al.*, 2000).

Ordovician quartz-rich metagreywacke from the Bendigo Zone

Sample VH2

This rock was recovered from a 19th century gold mine dump at Victoria Hill in Bendigo. The UTM Zone 55 location is 255341 5928864, and the rock type is a metagreywacke from the local Bendigonian stage (476.8 to 473.8) of the Ordovician Castlemaine Group. The zircon crystals are colourless, small, rounded and mostly prismatic, averaging ~120 × ~60 μm, but quite variable. The crystal shapes are mostly relatively simple, with prisms and one or two low pyramids; basal pinacoids are common. The more equant types show more complex forms involving multiple pyramids and prisms. The degree of rounding varies but is slight to moderate, with rare well-rounded individuals. Many grains contain up to 3 nested cores and, where possible (i.e. large enough), these was analysed. In nearly all cases, all parts of these grains show igneous-type oscillatory zoning, but a very few appear to have unzoned, possibly metamorphic cores, although these could simply represent cut effects. A few cores are also mottled and corroded, with oscillatory-zoned overgrowths.
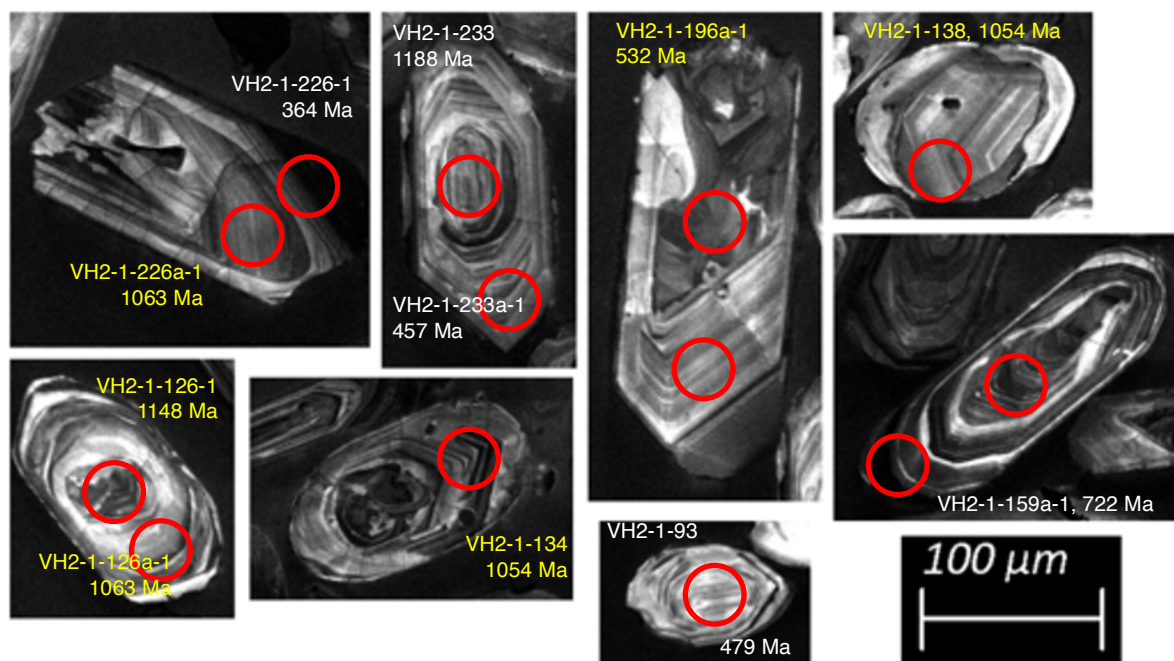

Figure A3.1. SEM-CL images of a selection of zircon grains from sample VH2.

Late Devonian I-type granitic rock from the Stawell Zone

Sample MB1

This is a coarse-grained, weakly peraluminous biotite granite from the Mount Bute pluton near the town of Lismore. The formal stratigraphic name is the Mount Bute Granite, and the location is 722538 5825533. Zircon crystals from this rock are very large and rather elongate, averaging ~300 × ~90 µm. They are colourless and somewhat translucent. Some have cracks and are irregularly iron-stained. The shapes are commonly simple, with prisms and a single low pyramid; very few pinacoids are developed. However, many crystals have multiple pyramids developed. Both cores and overgrowth rims display very fine, complex, oscillatory zoning. Most crystals have single, rather elongate and slightly to moderately well-rounded cores, although a few crystals have elongate nested cores, of two somewhat rounded individuals. A few cores also show mottled zoning and a few also have corroded (embayed) cores. Most cores are CL-bright and the most corroded examples are very CL-dark. A very few appear to have unzoned cores, but these may be due to cut effects.
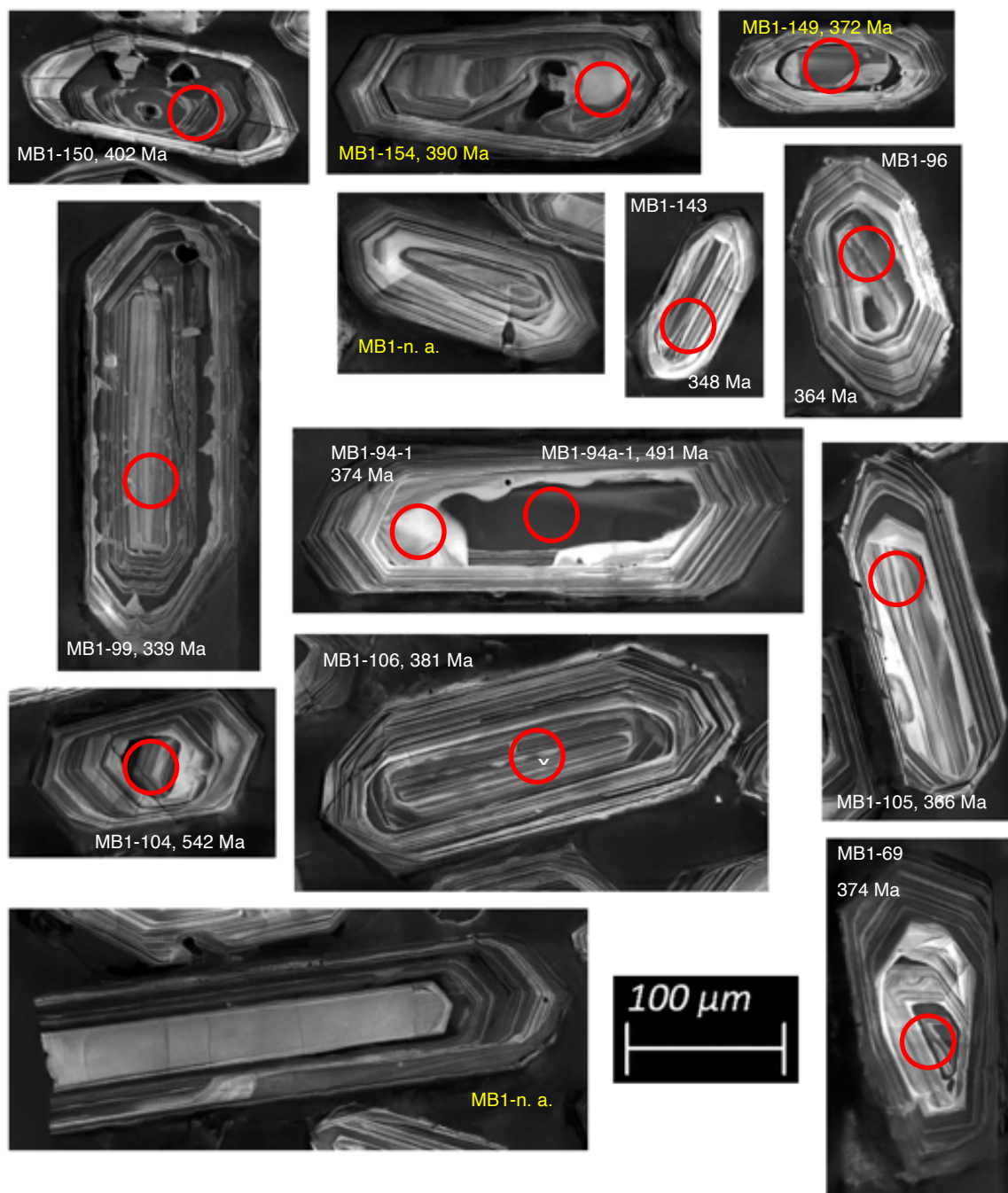
Figure A3.2. SEM-CL images of a selection of zircon crystals from sample MB1.

Late Devonian I-type granitic rocks of the Bendigo Zone

Sample AD1

This rock is a weakly peraluminous porphyritic micromonzogranite from the Mount Bolton pluton near the town of Addington. The formal stratigraphic designation is the Ercildoun Granite, and the sample location is 736107 5860516. The zircon crystals with distinct cores are relatively large and prismatic, with an average size of ~150 × ~50 μm. Their shapes dominantly involve long prisms and acute but commonly multiple pyramids, with few pinacoids. Distinct cores are large and abundant. They mostly have well rounded shapes and oscillatory zoning, although a good number show mottled zonation. Some are equant but most are somewhat elongate. Some show evidence of brittle fracture after having undergone some previous probable sedimentary rounding. The rims are narrow and also show typical igneous oscillatory zoning. Some cores are CL-dark and others CL-bright, and a few have embayed margins against the overgrowths.
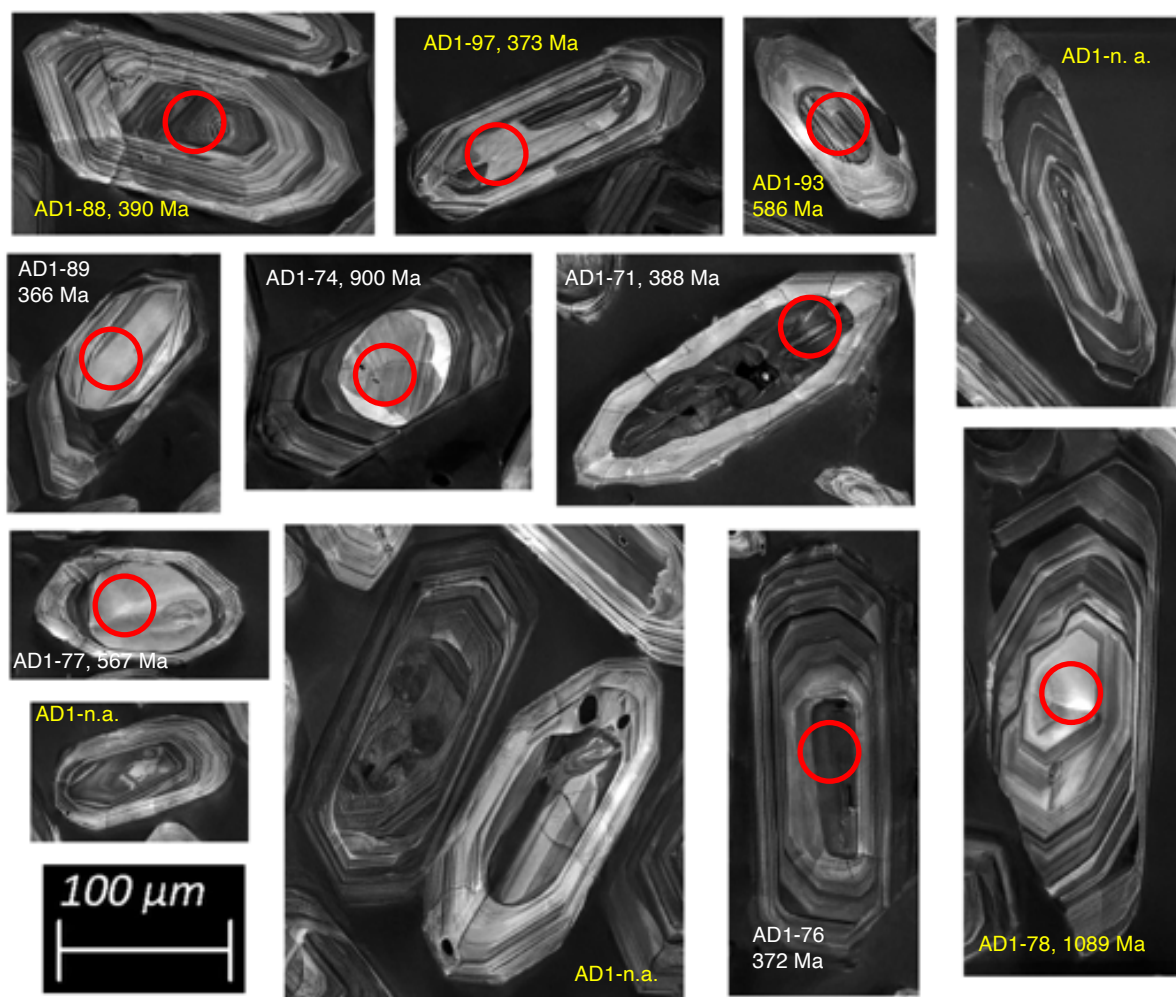
Figure A3.3. SEM-CL images of a selection of zircon crystals from sample AD1.

Sample HAR17 (H17)

This rock is somewhat transitional in character but is best regarded as S-type. It is from the Barringhup pluton of the Harcourt batholith, at location 237918 5903170. It is a strongly peraluminous, porphyritic micromonzogranite that contains biotite as the only major mafic mineral. The biotite is red-brown in thin section and the rock contains some very small grains of accessory almandine garnet. However, in some respects, the chemistry is rather more sodic than typical S-types, with K_2O/Na_2O = 1.21. This rock is the most 'S-type' of all samples taken from this batholith, which was described by Clemens (2018) as an I-type batholith built from magmas that had mainly metasedimentary source rocks with low degrees of chemical maturity — probably volcaniclastic arc greywackes. The zircon crystals from this sample are dominated by prism forms and are mostly capped by two or more pyramids. The zircon crystals are also rather more even in grain size than in many rocks examined in this study. The average dimensions are ~180 × ~65 µm — relatively elongate. Apparently inherited cores are common, quite large and mostly well rounded. Compared with their later magmatic over-growths many of the cores are relatively CL-dark and most have oscillatory zoning, as in the over-growths, although apparently unzoned cores are relatively common. Note that many well-rounded cores have spot ages very close to or identical with the previously determined magmatic age of 373 ± 2 Ma.
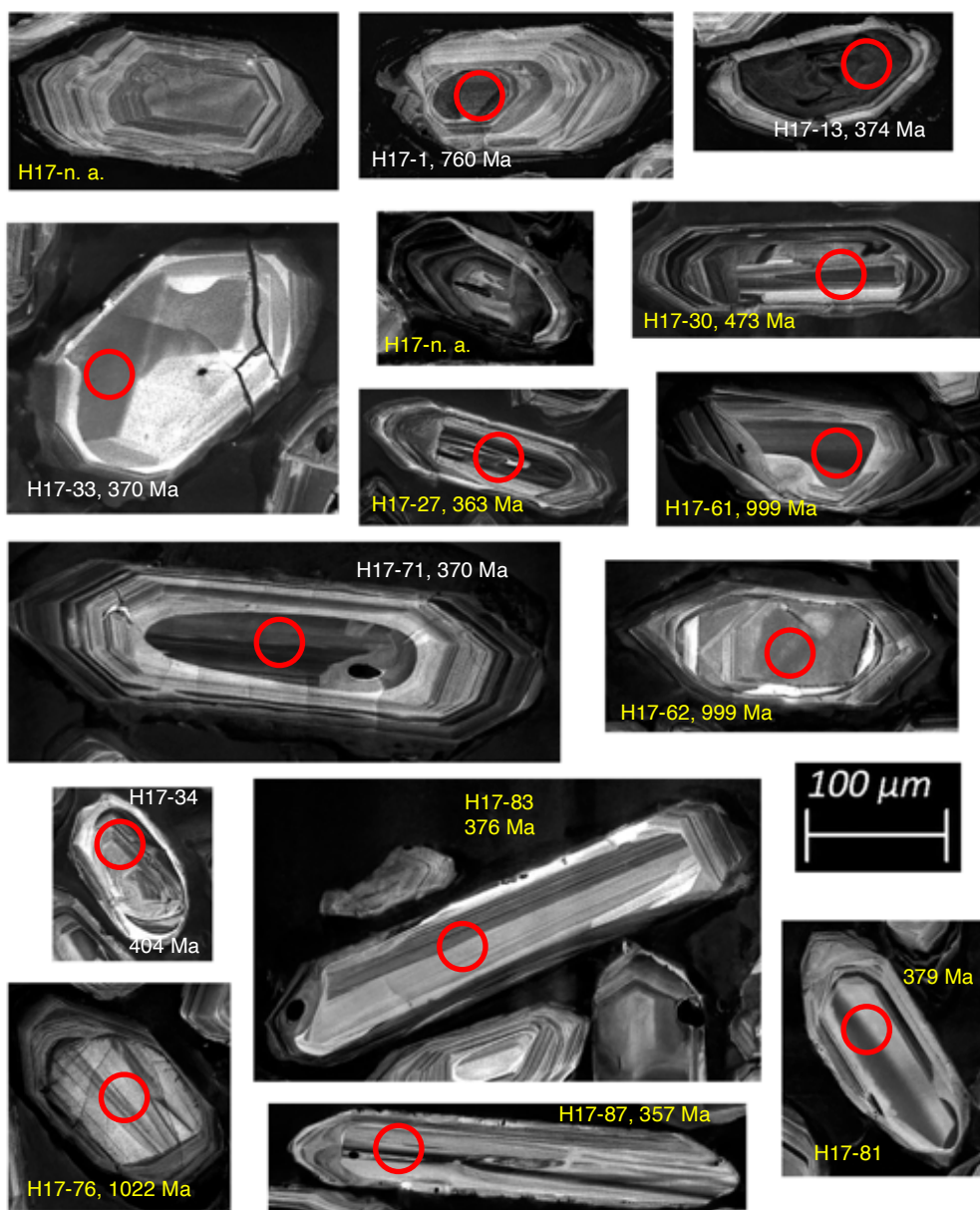
Figure A3.4. SEM-CL images of a selection of zircon crystals from sample HAR17.

Sample HAR19 (H19)

This sample is also from the Baringhup pluton, sampled at 765399 5903159, close to the Cairn Curran dam, and not far from the town of Baringhup itself. It is a weakly peraluminous biotite monzogranite that has more I-type character than sample HAR17 (H17). Its K_2O/Na_2O ratio is 1.14, the biotite is brown in thin section and there are no highly aluminous minerals present. The zircon crystals from this sample are quite variable in size, far more so than in sample HAR17 (H17), described above; they average ~130 × ~60 µm. They have fewer complex pyramid forms and seem dominated by simple prisms and pyramids. In other respects, the apparently inherited cores have very similar characteristics to those from zircon crystals in sample HAR17 (H17).
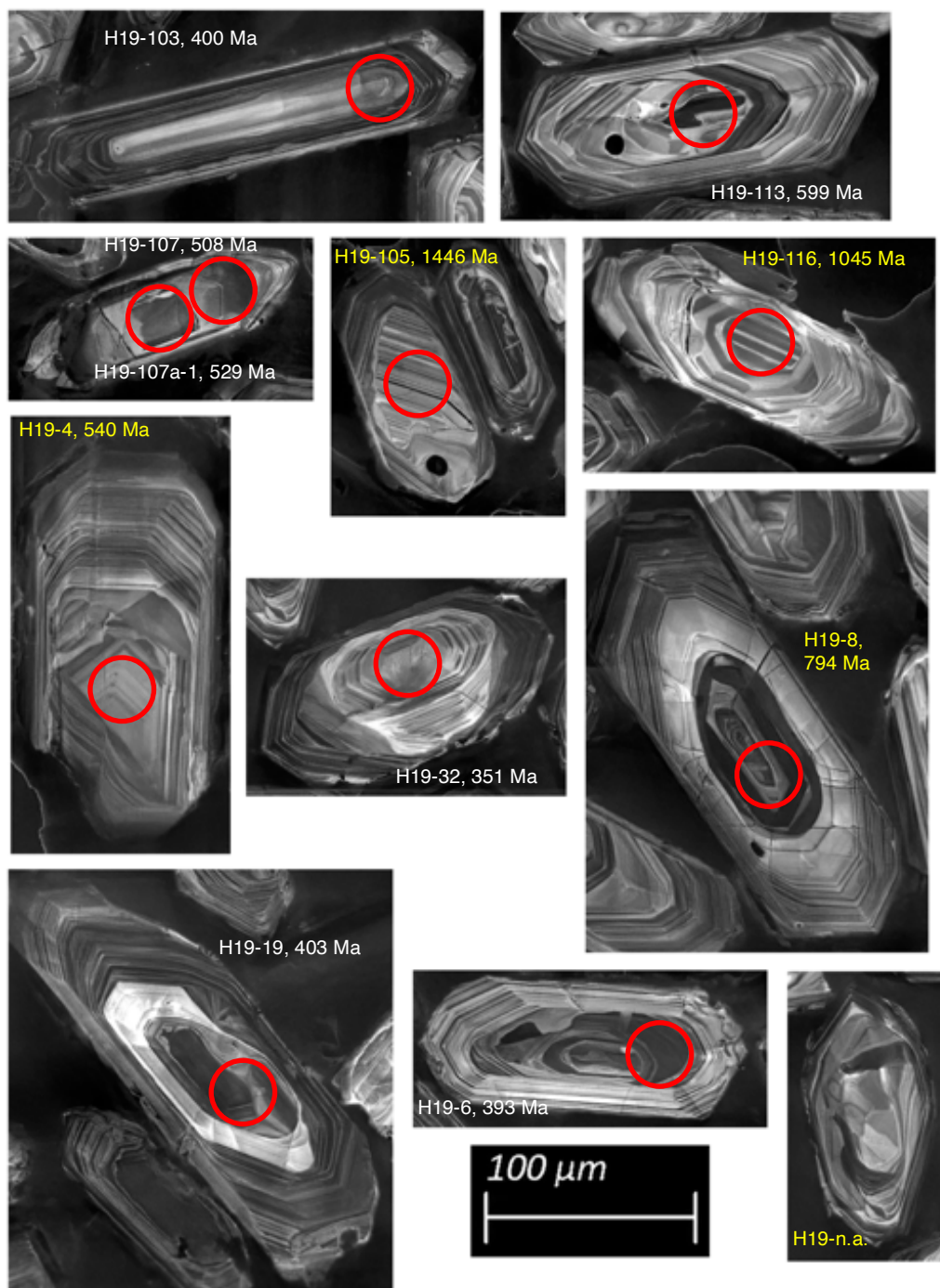
Figure A3.5. SEM-CL images of a selection of zircon crystals from sample HAR19.

Selwyn Block schistose metasedimentary xenolith from the Melbourne Zone

Sample S12

This sample is an amphibolite-facies metapelitic schist xenolith that has been inferred to be derived from the Selwyn Block, which forms the basement to the Melbourne Zone (Clemens & Phillips, 2014; Clemens & Buick, 2019). The sample was recovered from location 402318 5913611 near the summit of Mount Wombat in the eponymous pluton of the S-type Strathbogie batholith. The rock is well foliated, schistose and a finely stromatic migmatite. The melanosomes are composed of biotite, cordierite and quartz, with some sillimanite and hercynitic spinel, while the leucosomes contain quartz, plagioclase and alkali feldspar, with some subhedral to euhedral cordierite. The zircon yield from this sample was surprisingly low, and the zircon grains rather small and stubby, averaging ~65 × ~40 μm. They are colourless and moderately to well rounded, and those that show recognisable crystal forms appear to vary from relatively simple, with few facets, to grains with many complex forms. Many have distinct inner cores that are well rounded and either CL-dark or -bright. Igneous-type oscillatory zoning is essentially universal, except in very narrow, CL-bright overgrowths, which are interpreted to be of metamorphic origin. These are too narrow to date, but are assumed to be around 370 Ma, the usual date of granitic magma formation in the region.
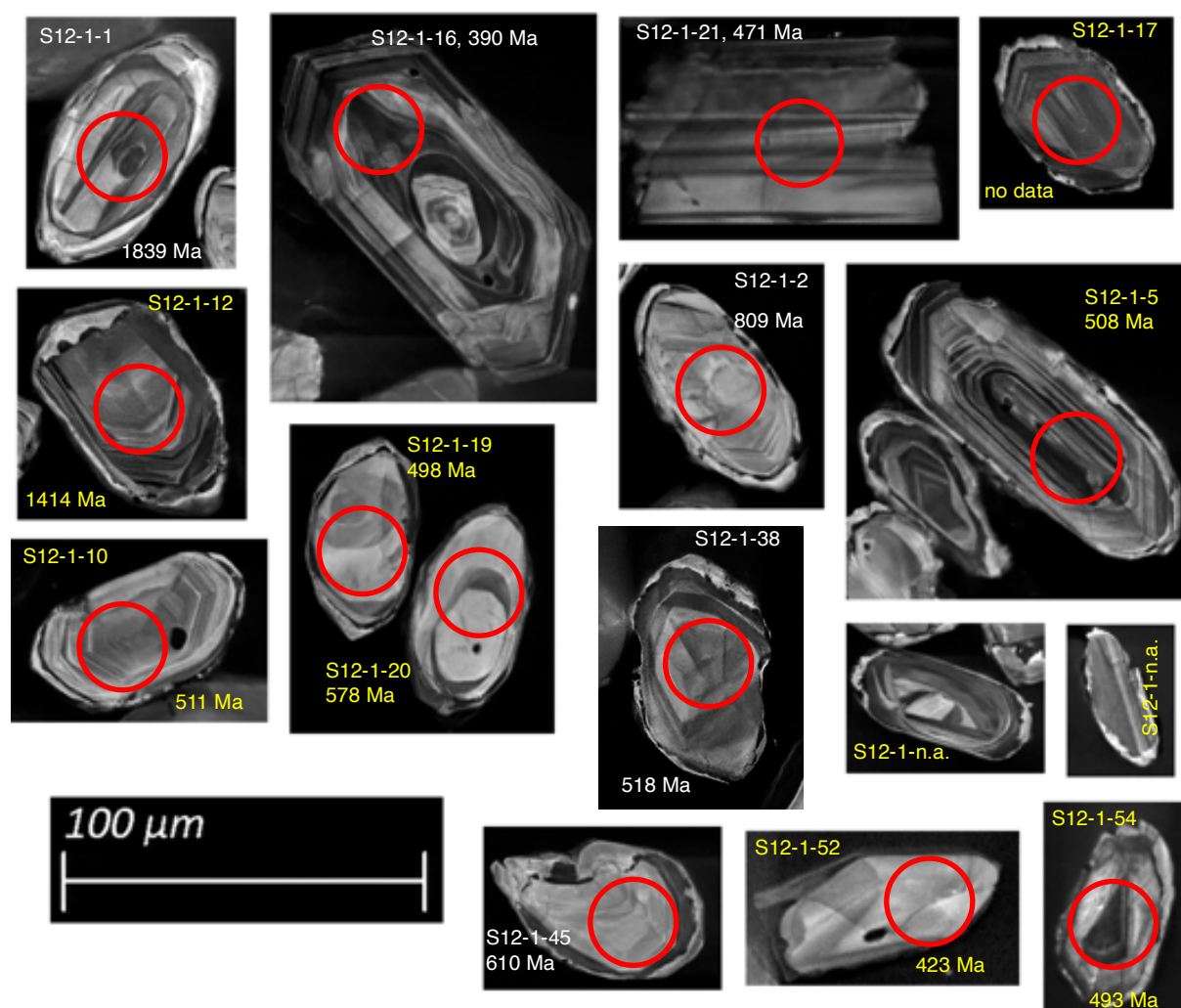
Figure A3.6. SEM-CL images of a selection of zircon grains from sample S12.

Late Devonian S-type granitic and volcanic rocks of the Melbourne Zone

Sample S1

This rock is a strongly peraluminous, porphyritic biotite–cordierite monzogranite from the Mount Wombat pluton of the Strathbogie batholith, collected at 343535 5887996, between the towns of Trawool and Kerrisdale. It is very similar in composition and texture to the host rock of the xenolith sample S12, described above. The zircon crystals from this sample are elongate and dominated by prism faces. The terminations are mostly single or double pyramids and a few have very small pinacoids. Some of the smaller, more equant zircon crystals have more complex habits. The average size is ~180 × ~90 µm. Apparent inherited cores are mostly large, quite abundant and vary in shape from moderately to well rounded. Embayments are common and most cores are CL-bright. They generally show complex oscillatory zoning, although a significant minority appear almost unzoned. Overgrowths are relatively narrow and show oscillatory zoning that appears weaker in amplitude than in most of the cores, due to the virtual absence of zones that are very CL-dark. Note that many distinct cores have spot ages close to the previously determined magmatic age of 374 ± 2 Ma.
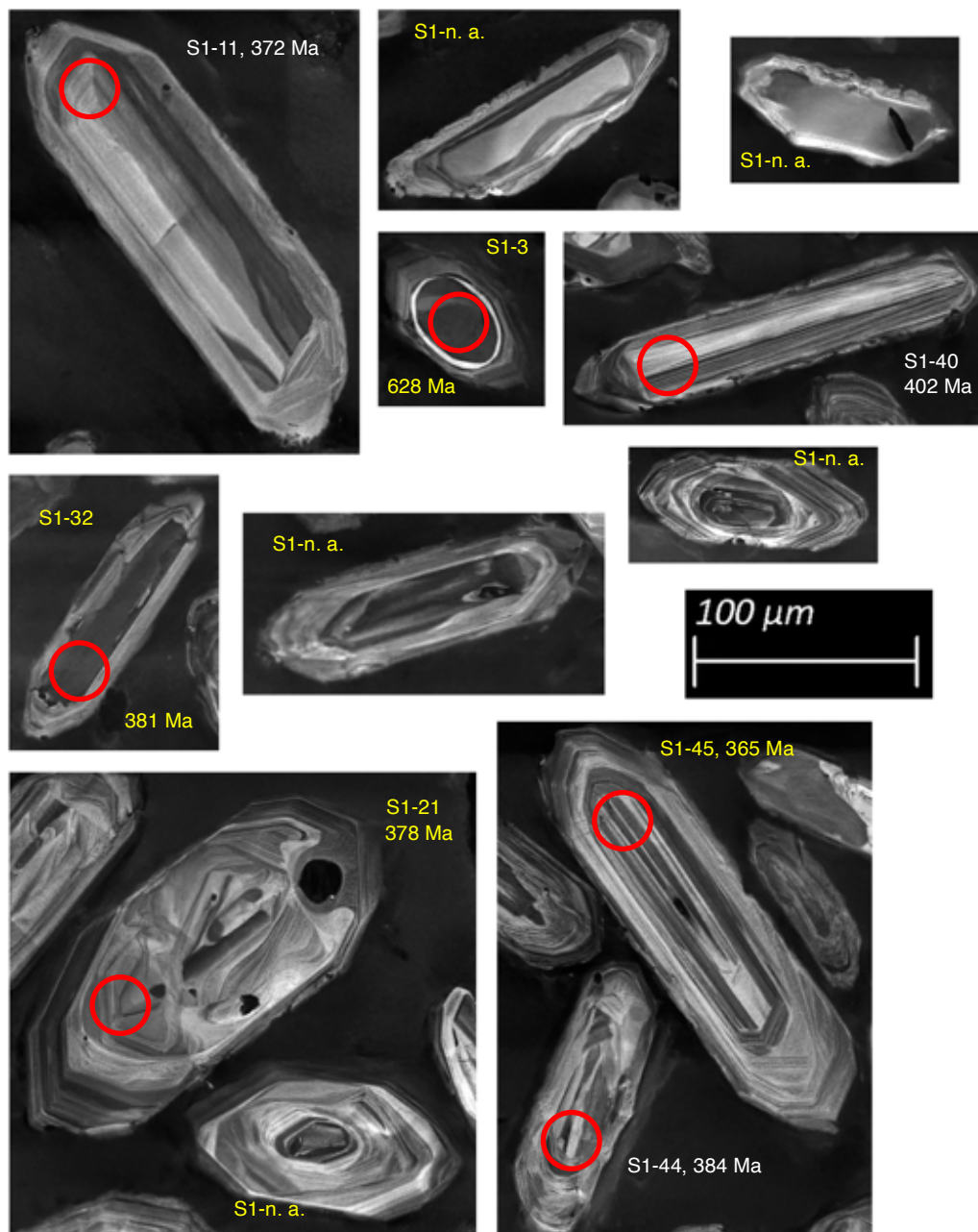
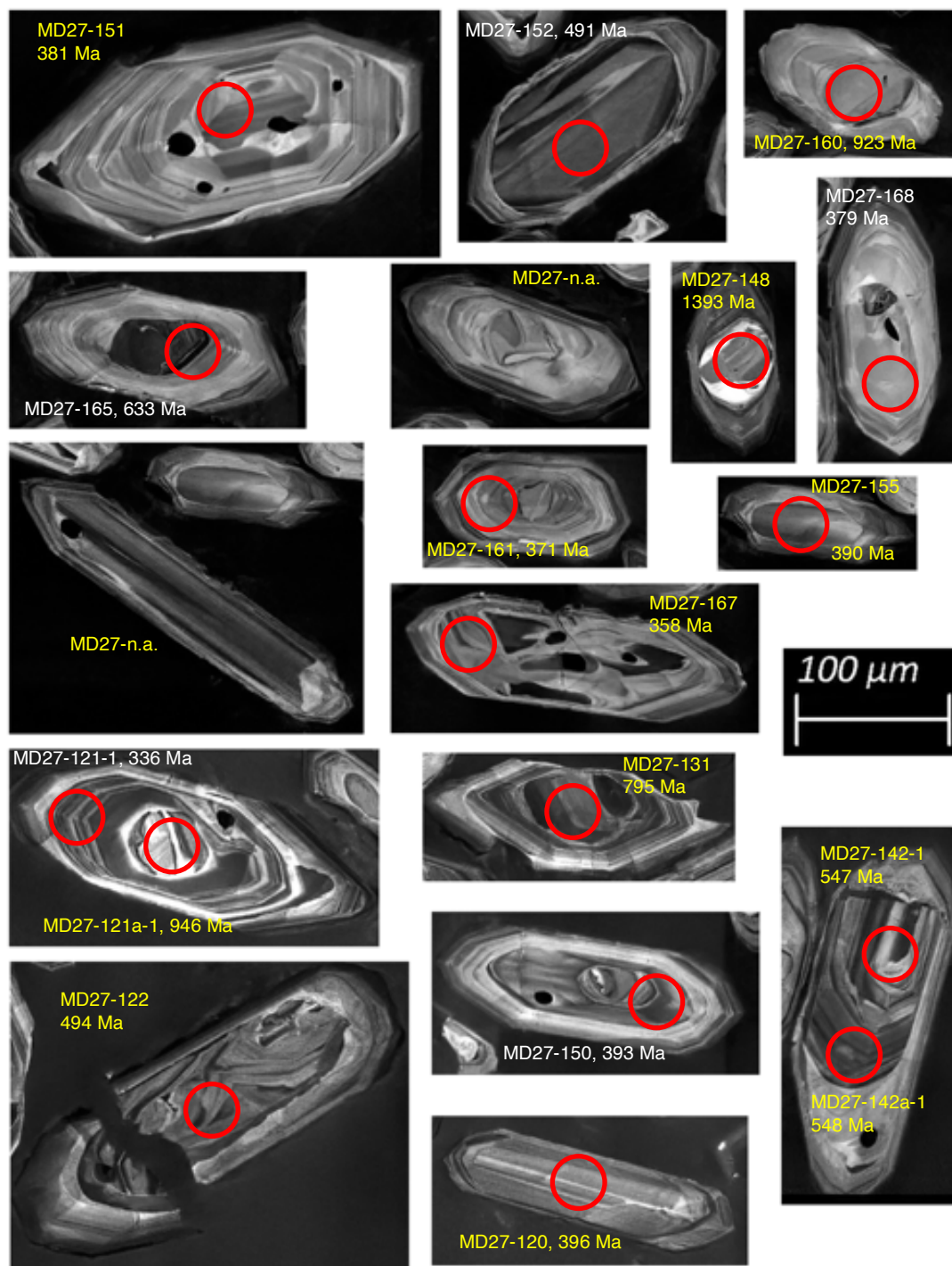**Figure A3.7.** SEM-CL images of a selection of zircon crystals from sample S1.

Sample MD27

This strongly peraluminous biotite granodiorite comes from the Mount Disappointment laccolith, at 333614 5860869. The biotite crystals in the rock are red-brown in colour, in contrast to the stronger red colour shown by the biotite in sample MD50, from the same pluton, and described below. The zircon crystals in MD27 are moderate in size, averaging ~145 × ~65 µm. The majority have multiple pyramid faces, but very few pinacoids are present. The majority have relatively large rounded cores with prominent oscillatory zoning, although some appear unzoned. In some cases, there are double cores, with inner rounded individuals enclosed within an outer rounded zone, all with oscillatory zoning. Corrosion and embayment of the distinct cores are common.

Figure A3.8. SEM-CL images of a selection of zircon crystals from sample MD27.

Sample MD50

This is a seriate-textured, strongly peraluminous biotite granodiorite from the Mount Disappointment laccolith, collected at 333119 5858567. The rock is more highly peraluminous that sample MD27, described above and contains biotite crystals that are redder in thin-section colour. The zircon crystals from this rock are more homogeneous in size range and generally larger than in MD27, averaging ~175 × ~80 µm. The crystals are mostly colourless, but some are pale brown. The forms are quite similar to those for the zircon in MD27. Some of the smallest and most equant crystals have almost no prism faces developed. The distinct cores are typically large and moderately to well rounded, although a minority show brittle fracture surfaces. The majority of the cores in this sample are quite CL-dark, which is in contrast with those from MD27, in which the cores and rims both show ranges of tone in the mid-grey range. Apparently unzoned cores are less common in MD50 and embayments and corrosion are very uncommon features, which also contrasts with the zircon crystals in MD27.
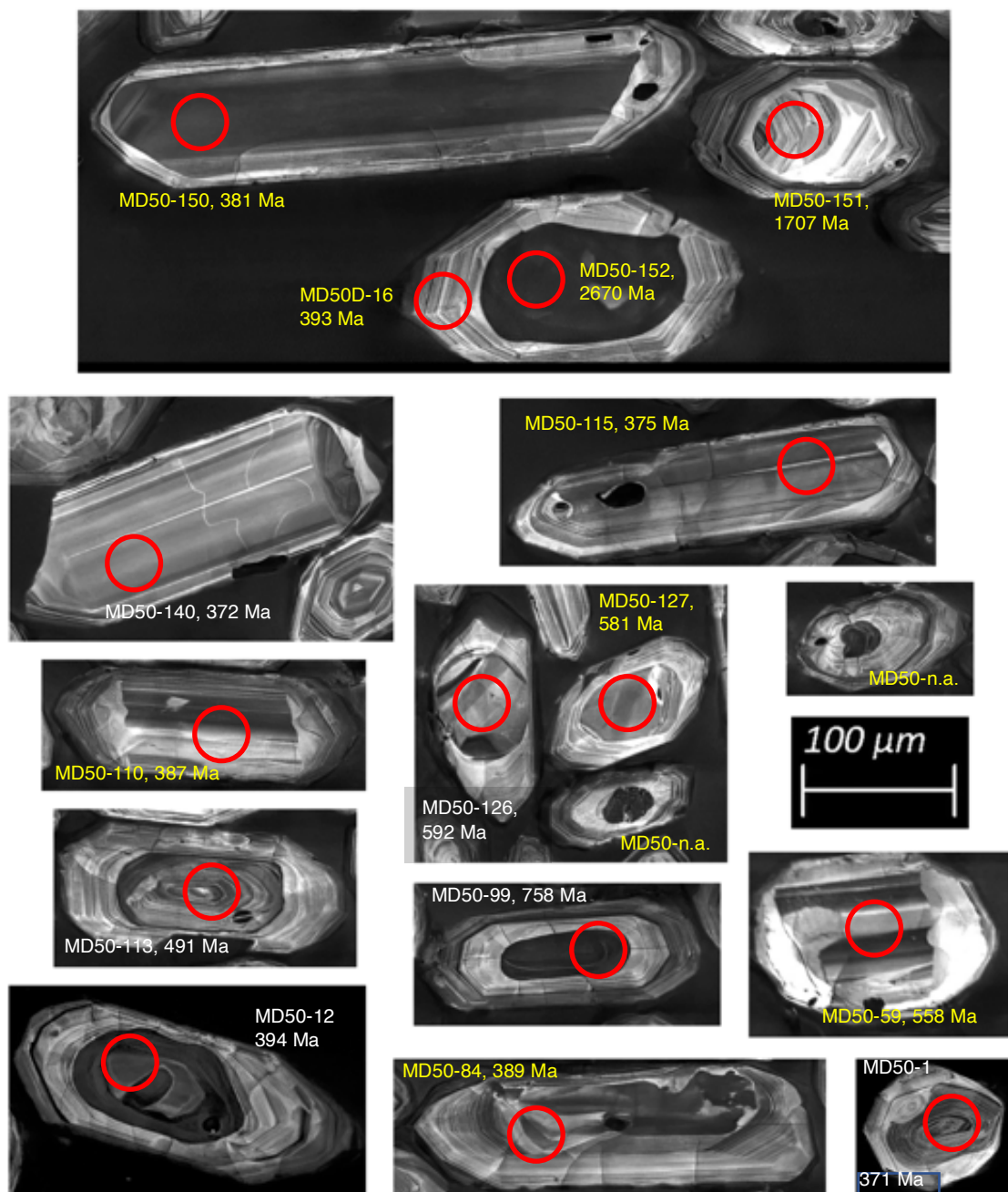
Figure A3.9. SEM-CL images of a selection of zircon crystals from sample MD50.

Late Devonian I-type granitic rocks of the Melbourne Zone

Sample L1

This is a high-K, metaluminous, hornblende–biotite granodiorite from the Lysterfield pluton in the Dandenong Ranges Igneous Complex, collected from Lysterfield Quarry at 348149 5800013, on the ESE edge of the Melbourne suburb of Rowville, in the city of Knox. The yield of zircon from this rock was lower than from other granitic rocks in this study, and the crystals are somewhat smaller, averaging 130 × 40 µm. They are dominated by simple prisms and single pyramids, but basal pinacoids are also common. Presumed inherited cores are abundant but commonly smaller in size than in any of the other granitic samples described above. The core shapes are mostly well-rounded but angular, broken types are also present, along with some showing significant corrosion and embayment, as in many of the rocks studied here. As in most other rocks in the study, the L1 zircon crystals and their cores show complex oscillatory zoning, although some of the CL-dark cores, particularly, appear unzoned.
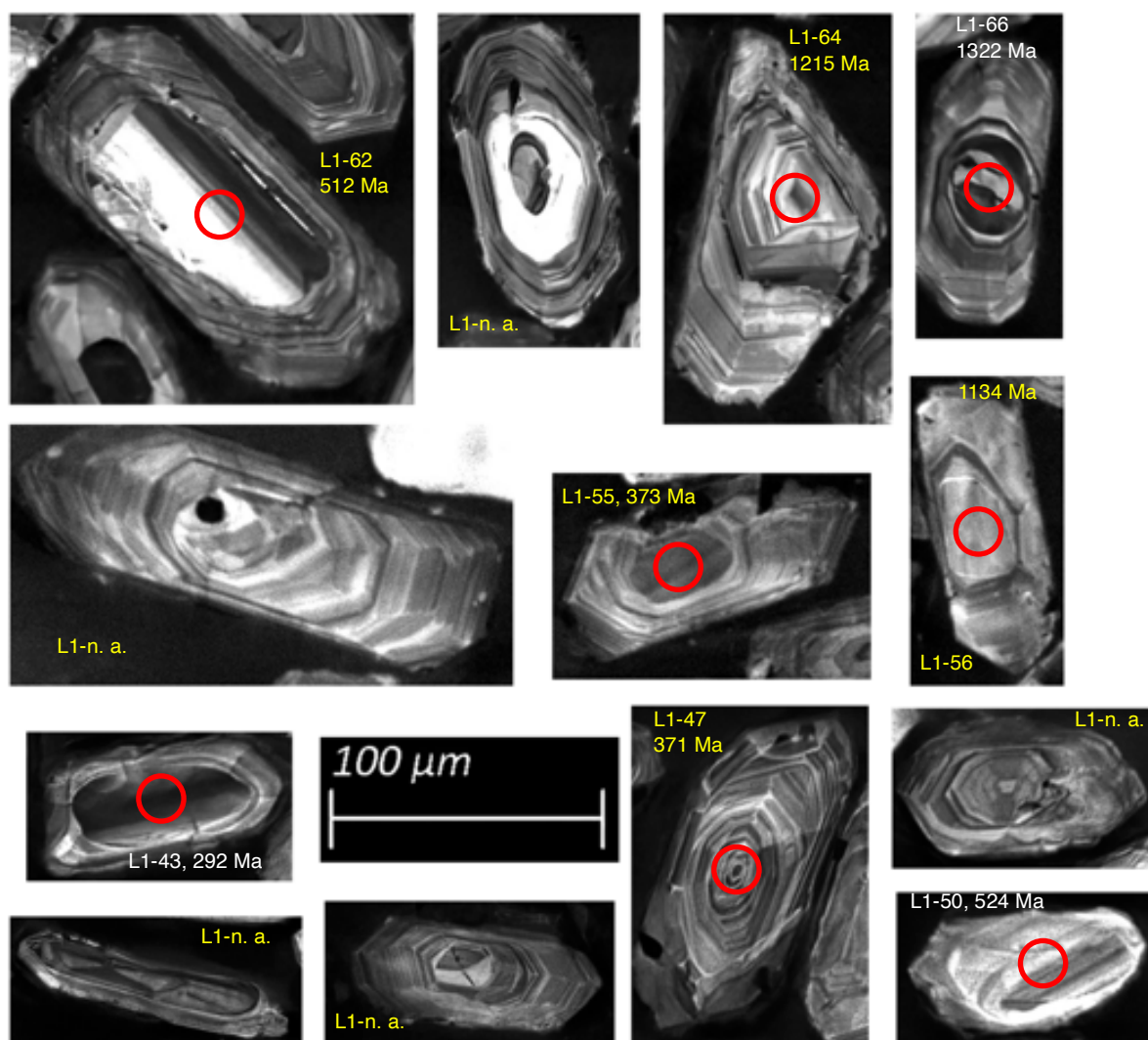
Figure A3.10. SEM-CL images of a selection of zircon crystals from sample L1.

Sample TY2

This rock is a very weakly peraluminous porphyritic hornblende–biotite microgranite collected from the inner, low-Al part (Clemens *et al.*, 2016) of the Tynong pluton in the eponymous batholith. The location is the Tynong quarry operated by Fulton Hogan, at 379292 5786766, near the town of Tynong North. The average size of the zircon crystals in this sample is ~170 × 70 μm. Both the zircon yield and the crystal size are higher than in the nearby Lysterfield pluton, as exemplified by sample L1, described above. Crystal forms vary but are dominated by prisms and single pyramids. Crystals with 2 pyramids are uncommon, and a very few have basal pinacoids. The possibly inherited cores are much larger than those in L1 but otherwise very similar in their shapes and twinning characteristics.
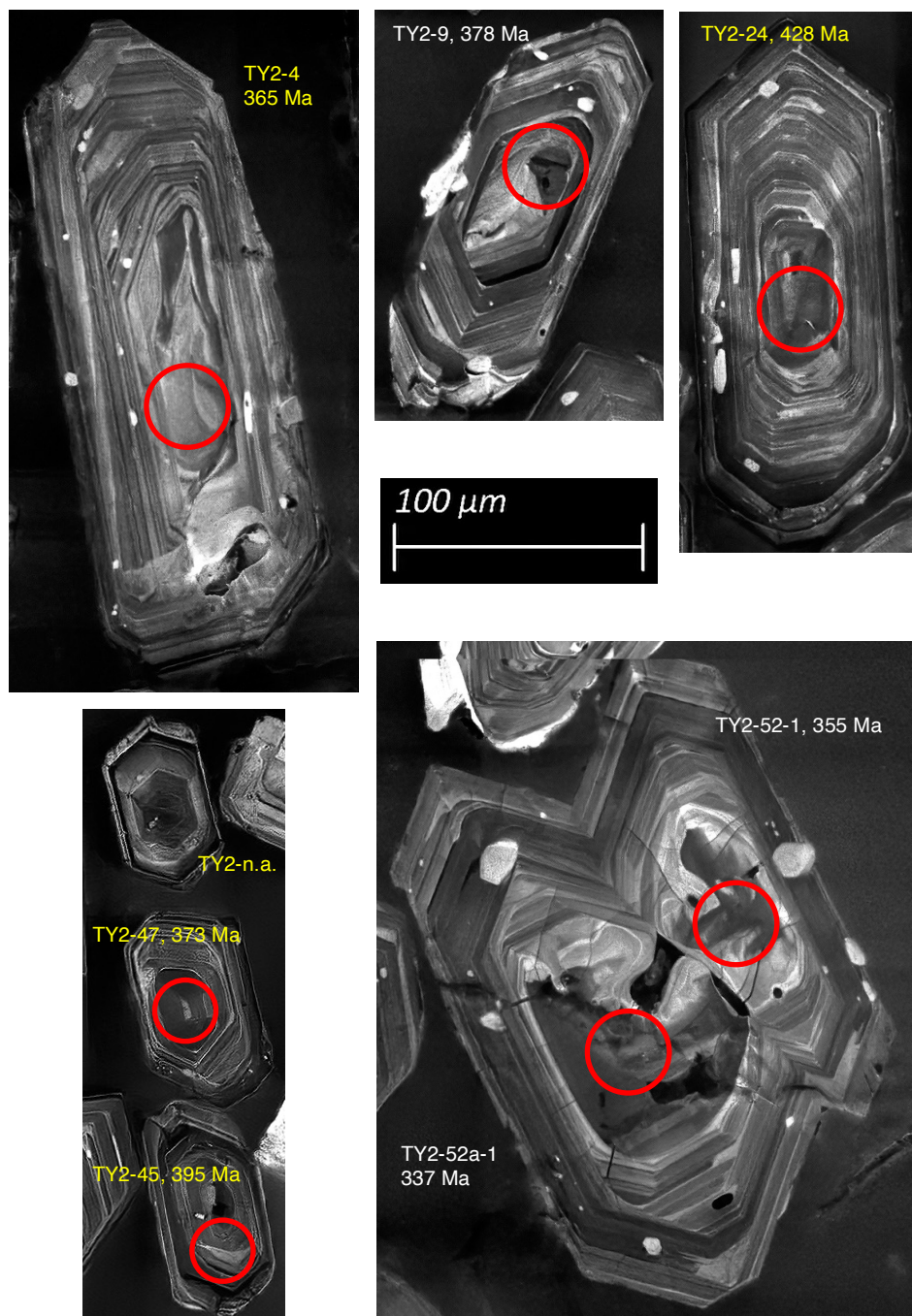
Figure A3.11. SEM-CL images of a selection of zircon crystals from sample TY2.

Early Devonian S-type granite from the Bassian Basement Terrane

Sample WPB7 (PS)

This is a garnet- and biotite-rich mafic schliere (a flow segregated cumulate layer) from the Norman Point biotite monzogranite (NPBM) unit in the Oberon pluton of the *ca* 395 Ma Wilsons Promontory batholith. It was collected from Squeaky Beach, north of Pillar Point, at about 440011 5679851. As described by Wallis and Clemens (2018) and Clemens *et al.* (2020), this rock represents a natural concentration of mafic and accessory minerals from the NPBM magma, and was therefore chosen as likely to have a high zircon yield. The zircon crystals in this sample are relatively large, with average dimensions of ~180 × ~80 µm. Prisms dominate, with terminations of two prominent pyramids typical, although simple pyramids are also relatively abundant. Pinacoids are very scarce. The distinct cores are quite large in this sample, with some nested cores also present. These cores tend to be quite well rounded and embayments and corrosion are relatively common. Oscillatory zoning is common in both cores and overgrowths but there are numerous examples of cores that appear unzoned, although some of these could represent cut effects. Most crystals have moderate CL contrast levels, with mid-grey tones dominant in both cores and overgrowths.
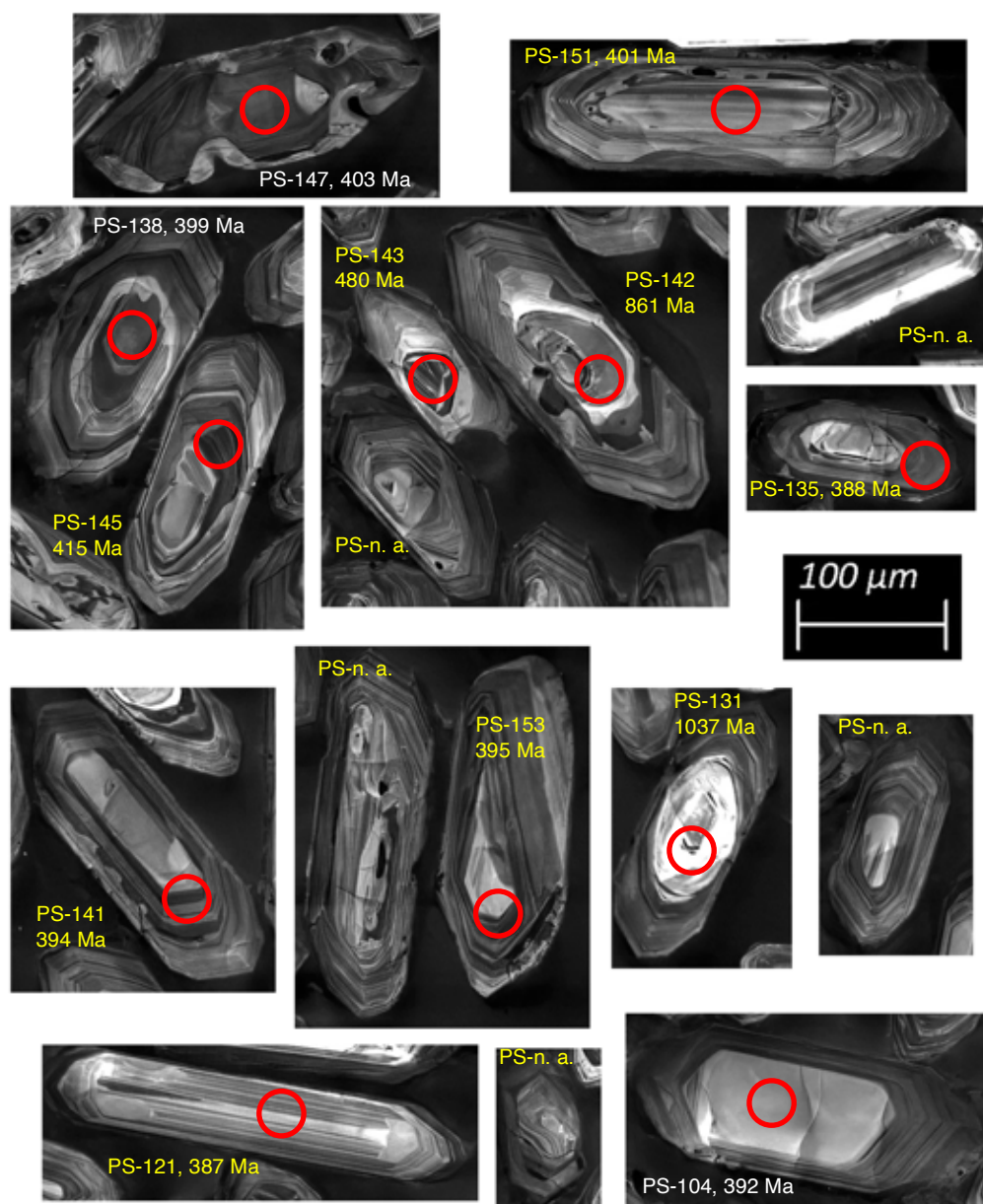
Figure A3.12. SEM-CL images of a selection of zircon crystals from sample WPB7.

17

Zircons in additional samples from the Melbourne Zone and the boundary with the Tabberabbera Zone
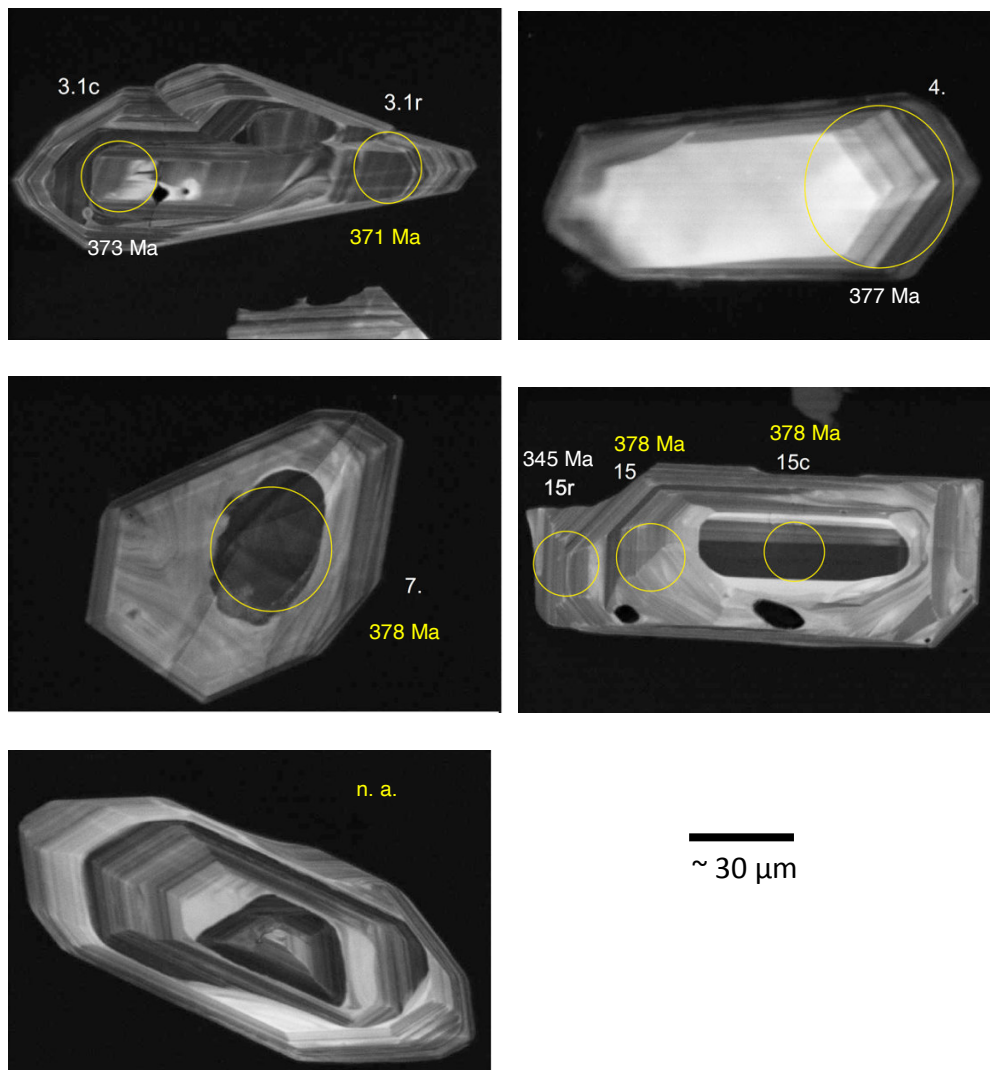
A-type Toombullup Ignimbrite sample TOOM

Fig. A3.13. SEM CL images of a selection of zircon crystals from sample TOOM. Some of these images formed parts of figure 5 of Clemens *et al.* (2014), and the labelled circles represent spots dated in that study. Note the presence of distinct and commonly rounded CL-darker cores in many of these crystals. The dating of Clemens *et al.* (2014) showed that these cores have the same age, within uncertainty, as the rims. Thus, these are interpreted as early-formed autocrysts, rather than inherited detrital grains. This interpretation is consistent with the high-temperature, A-type character of the host magma.

S-type Lake Mountain ignimbrite sample E27-2
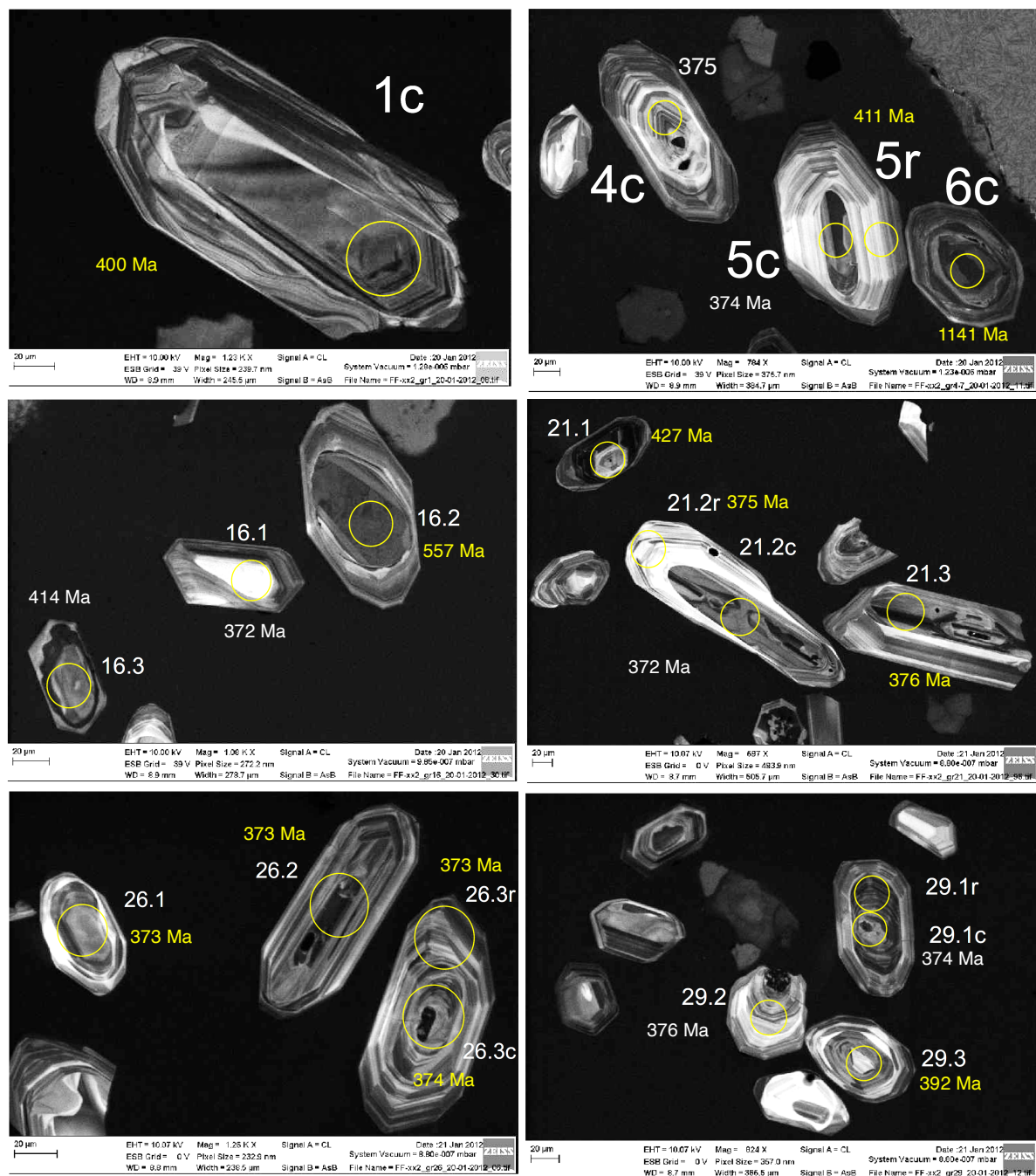
Fig. A3.14. SEM CL images of a selection of zircon crystals from sample E27-2. The numbered yellow circles represent analysed spots. Note that many crystal cores were targeted, even though the sample was analysed with a view toward dating magmatic crystallisation.

References

Clemens, J. D. (2018). Granitic magmas with I-type affinities, from mainly metasedimentary sources: the Harcourt batholith of southeastern Australia. *Contributions to Mineralogy and Petrology, 173*(11), 93. https://doi.org/10.1007/s00410-018-1520-z

Clemens, J. D., & Buick, I. S. (2019). Proterozoic VanDieland in central Victoria: ages, compositions and source depths for Late Devonian silicic magmas. *Australian Journal of Earth Sciences, 66*(4), 519–530. https://doi.org/10.1080/08120099.2018.1554603

Clemens, J. D., & Phillips, G. N. (2014). Inferring a deep crustal source terrane from a high-level granitic pluton: the Strathbogie batholith, Australia. *Contributions to Mineralogy and Petrology, 168*(5), 1070. https://doi.org/10.1007/s00410-014-1070-y

Clemens, J. D., Regmi, K., Nicholls, I. A., Weinberg, R., & Maas, R. (2016). The Tynong pluton, its mafic synplutonic sheets and igneous microgranular enclaves: the nature of the mantle connection in I-type granitic magmas. *Contributions to Mineralogy and Petrology, 171*(4), 1–17. https://doi.org/10.1007/s00410-016-1251-y

Clemens, J. D., Stevens, G., le Roux, S., & Wallis, G. L. (2020). Mafic schlieren, crystal accumulation and differentiation in granitic magmas: an integrated case study. *Contributions to Mineralogy and Petrology, 175*(5), 51. https://doi.org/10.1007/s00410-020-01689-x

VandenBerg, A. H. M., Willman, C. E., Maher, S., Simons, B. A., Cayley, R. A., Taylor, D. H., Morand, V. J., Moore, D. H., & Radojkovic, A. (2000). *The Tasman Fold Belt System in Victoria*. Melbourne: Geological Survey of Victoria Special Publication.

Wallis, G. L., & Clemens, J. D. (2018). Geology and field relations of the Wilsons Promontory batholith, Victoria: multiple, shallow-dipping, S-type, granitic sheets. *Australian Journal of Earth Sciences, 65*(6), 769–785. https://doi.org/10.1080/08120099.2018.1472142

Supplementary Paper 4

A selection of Wetherill concordia plots for analysed granitic, metamorphic and sedimentary rocks

The plots below show concordia diagrams for some critical sections of the age spectra displayed by the cores of inherited or detrital zircon crystals in the various rocks. See the main document and Figures 5 to 10 for further information. Note that only spots with between 90 and 110% concordance were plotted here and used in the probability density distribution (PDD) analysis of age peaks. The right-hand vertical axes portray the degrees of concordance as colour coding applied to the 2σ error ellipses.
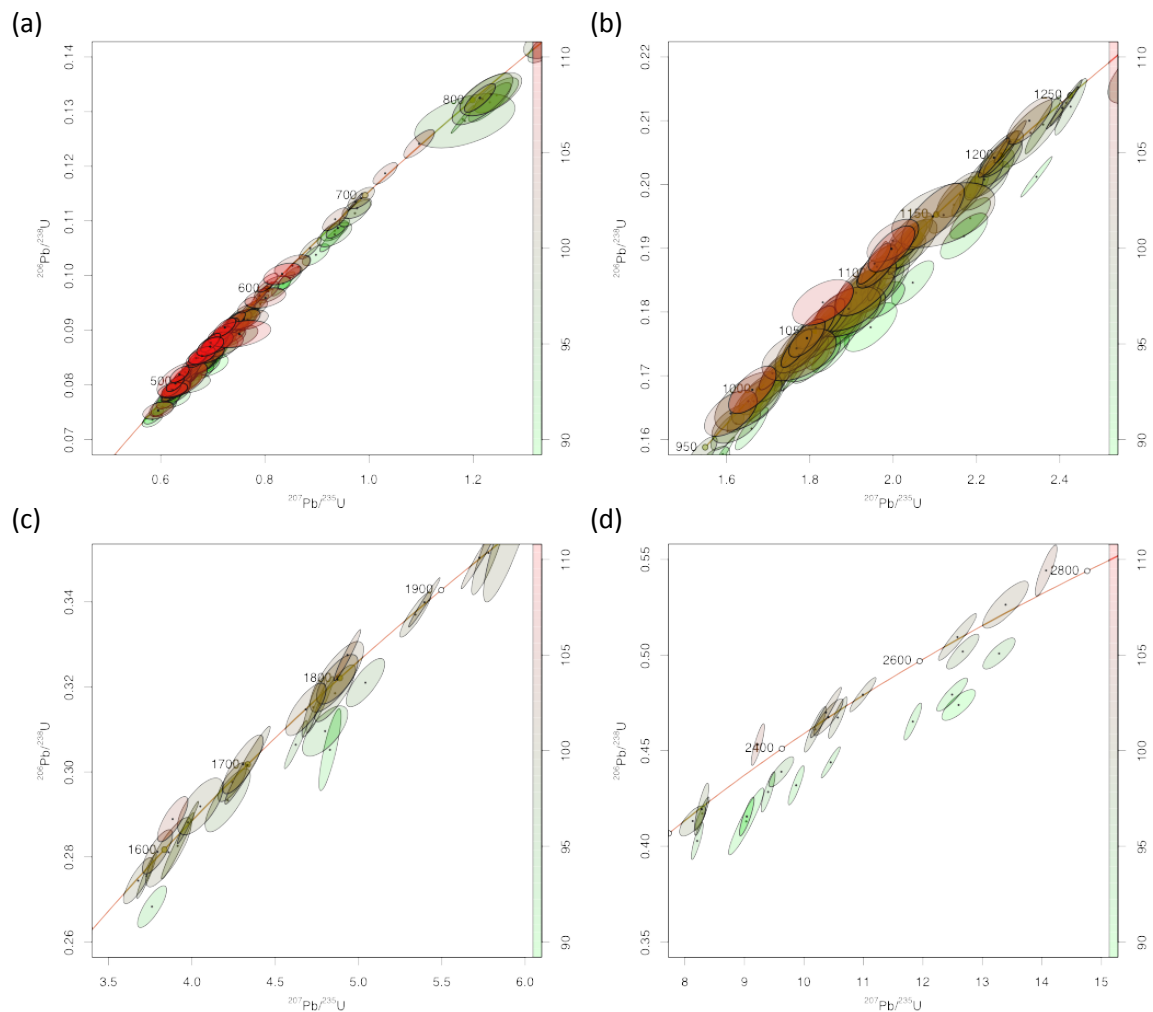
Figure A4.1. Wetherill concordia plots for detrital zircon in Bendigo Zone Ordovician metagreywacke VH2. There are 363 concordant spots and the illustrated panels are: (a) for 400 to 800 Ma, (b) for 950 to 1250 Ma, (c) for 1600 to 1900 Ma and (d) for 2000 to 2800 Ma. Age peaks identified in the PDD analysis are at: 524, 804, 869, 1049, 1364, 1624, 1779, 1944, 2024, 2244, 2479, 2634, 2729, 2799 and 2999 Ma.
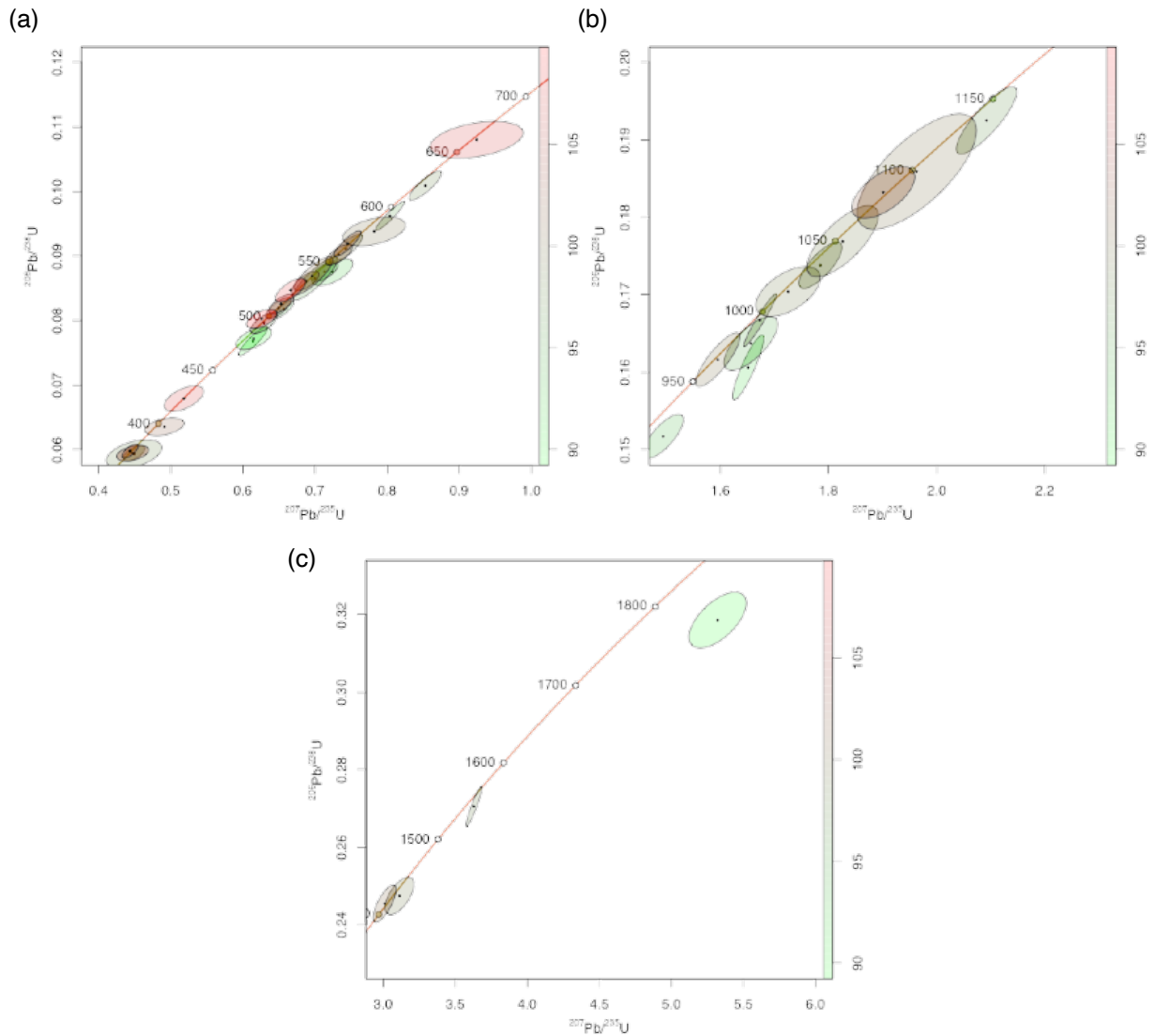
Figure A4.2. Wetherill concordia plots for zircon in Selwyn Block Cambrian metapelitic xenolith S12. There are 40 concordant spots and the illustrated panels are: (a) for 400 to 700 Ma, (b) for 950 to 1150 Ma and (c) for 1400 to 1800 Ma. Age peaks identified in the PDD analysis are at: 534, 789, 989, 1424,1549, 1784, 3399 and 3534 Ma. Ages younger than 534 Ma represent metamorphism associated with the formation of the host granitic magma.
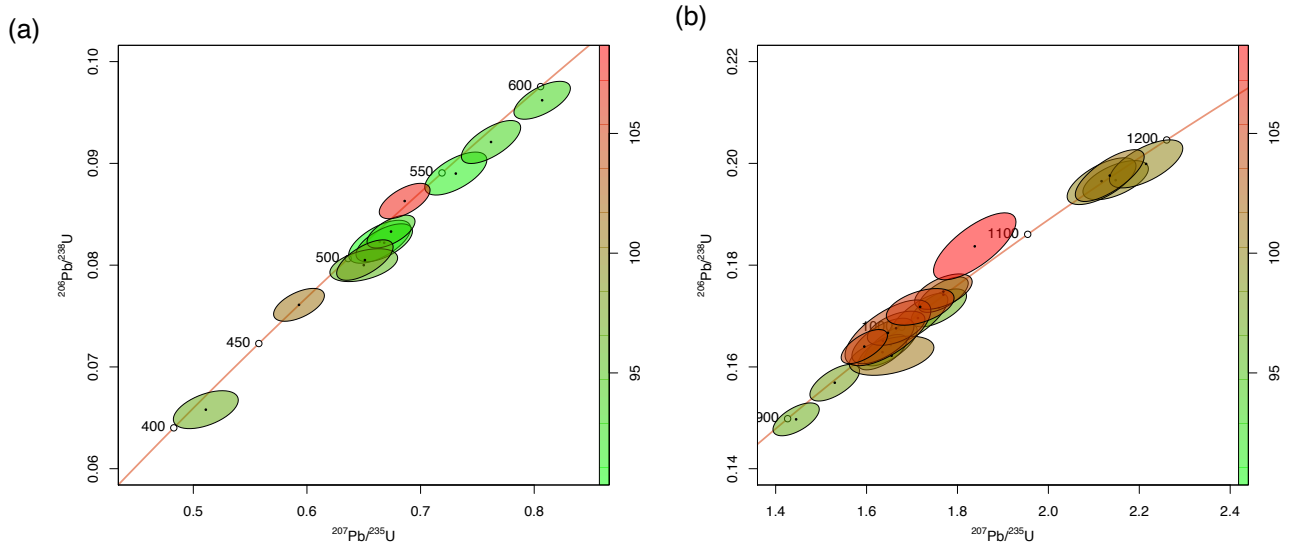
Figure A4.3. Wetherill concordia plots for inherited zircon in the Late Devonian, S-type monzogranite HAR17 from the Mount Alexander pluton of the Harcourt batholith. There are 33 concordant spots and the illustrated panels are: (a) for 400 to 600 Ma and (b) for 900 to 1200 Ma. Age peaks identified in the PDD analysis are at: 414, 519, 999, 1164, 1704, 2019 and 2239 Ma.
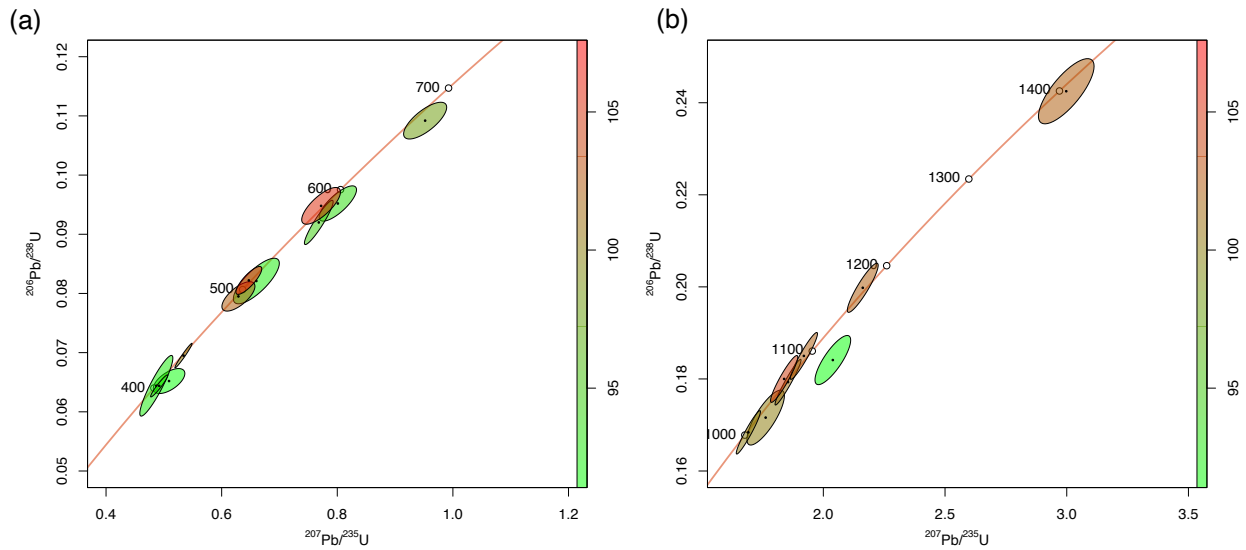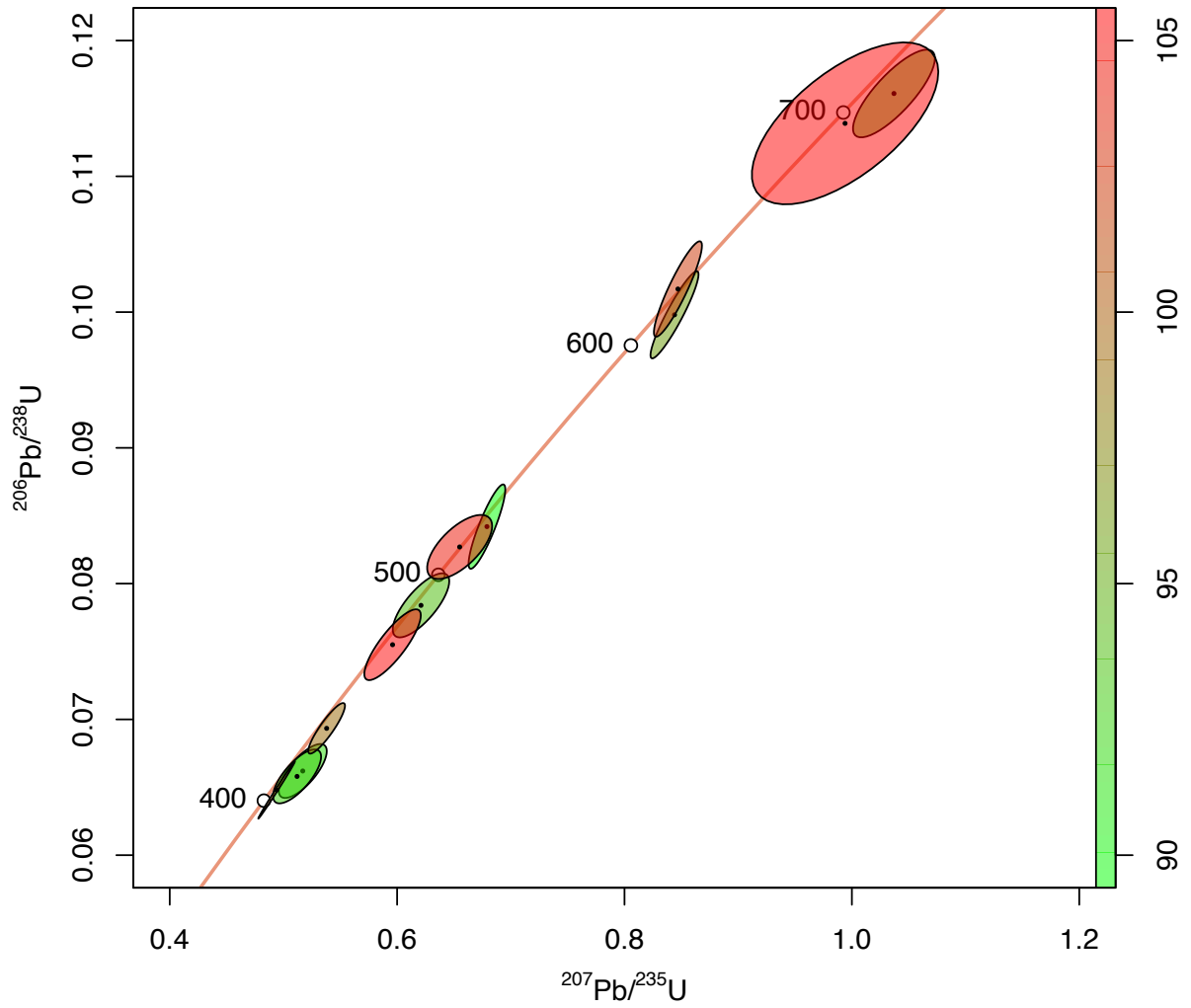

Figure A4.4. Wetherill concordia plots for inherited zircon in the Late Devonian, I-type porphyritic monzogranite AD1 from the Ercildoun Granite. There are 22 concordant spots and the illustrated panels are: (a) for 400 to 700 Ma and (b) for 1000 to 1400 Ma. Age peaks identified in the PDD analysis are at: 414, 509, 579, 669, 1079,1169, 1404, 1724, 2579 and 2709 Ma.

Figure A4.5. Wetherill concordia plot for inherited zircon in the Late Devonian, I-type Lysterfield Granodiorite sample L1. There are 16 concordant spots and illustrated panel is for 400 to 700 Ma. Age peaks identified in the PDD analysis are at: 424, 494, 629, 704, 1144 and 1734 Ma.
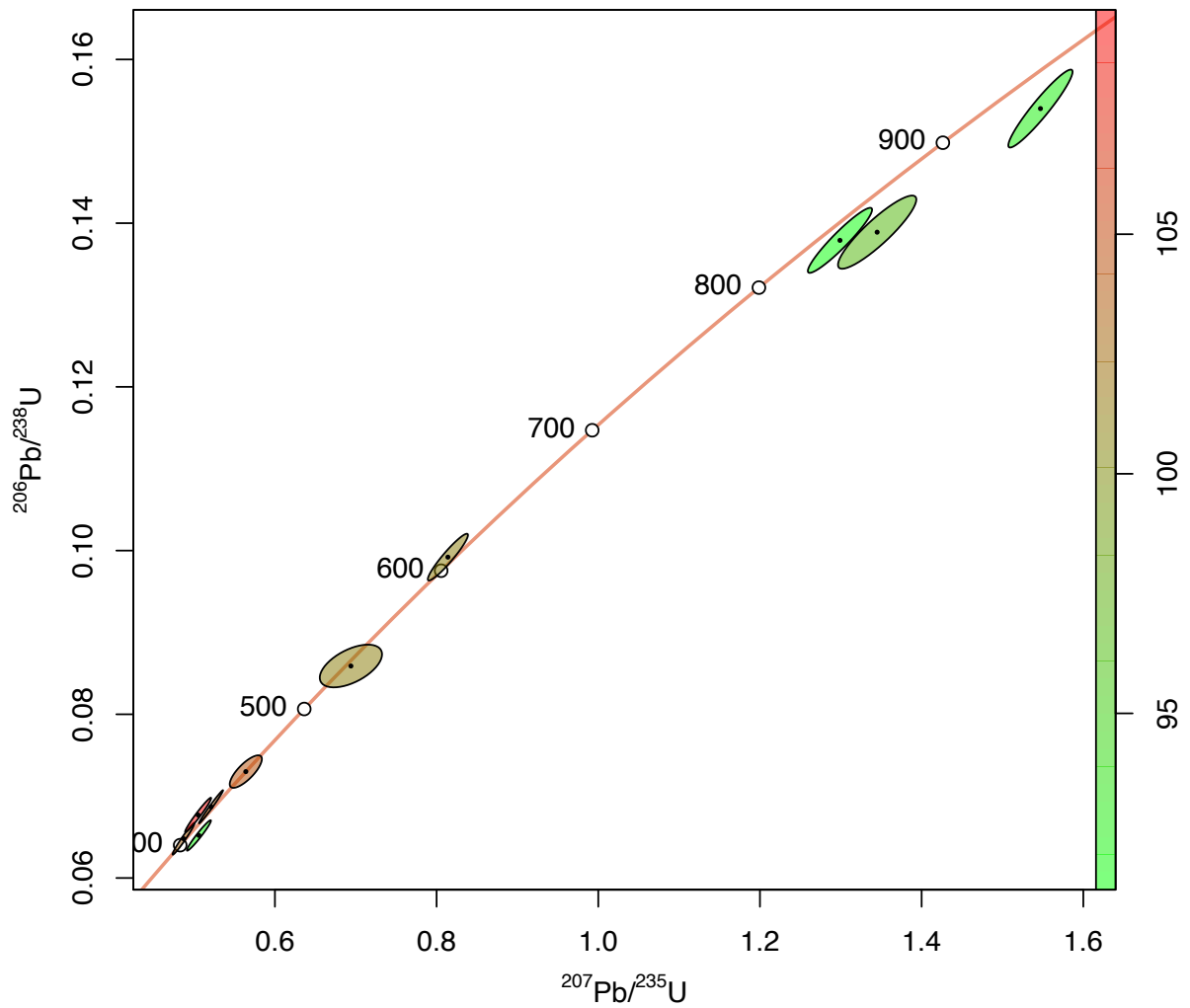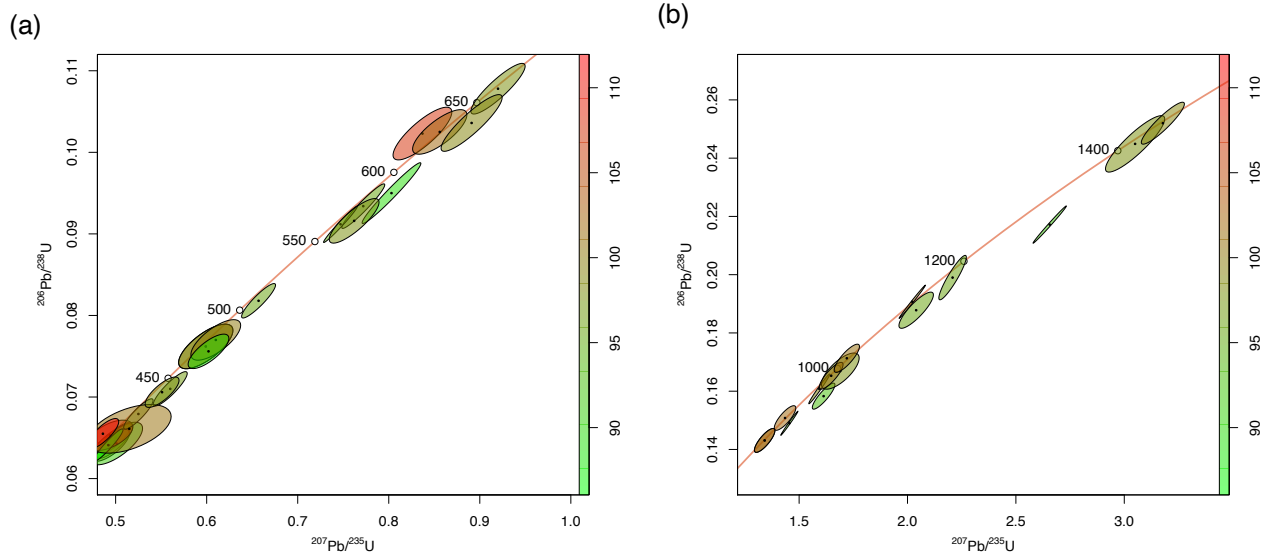
Figure A4.6. Wetherill concordia plot for inherited zircon in the Late Devonian, I-type monzogranite from the Tynong pluton of the Tynong batholith, sampleTY2. There are 23 concordant spots and the illustrated panel is for 400 to 900 Ma. Age peaks identified in the PDD analysis are at: 429, 534, 614, 844 and 924 Ma.

Figure A4.4. Wetherill concordia plots for inherited zircon in the Late Devonian, S-type monzogranite S1 from the Mount Wombat pluton of the Strathbogie batholith. There are 35 concordant spots and the illustrated panels are: (a) for 400 to 700 Ma and (b) for 900 to 1500 Ma. Age peaks identified in the PDD analysis are at: 424, 584, 634, 979, 1129, 1274, 1434, 1724, 2444, 2834 and 3014 Ma.
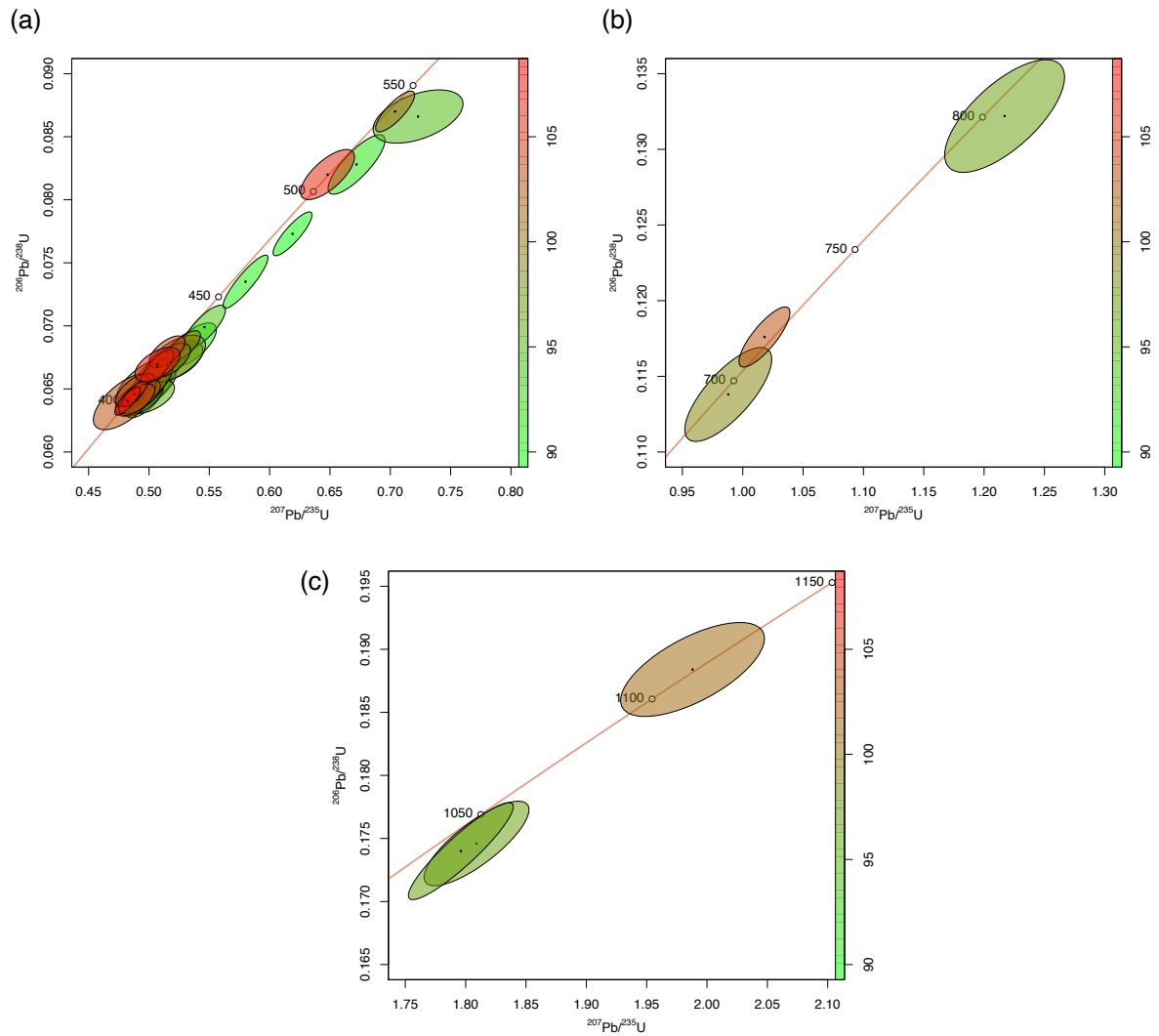
Figure A4.8. Wetherill concordia plots for inherited zircon in the Early Devonian, S-type, garnet-rich schliere segregation, sample WPB7 from the Norman Point biotite monzogranite in the Oberon pluton of the Wilsons Promontory batholith. There are 35 concordant spots and the illustrated panels are: (a) for 400 to 550 Ma and (b) for 700 to 800 Ma and (c) for 1050 to 1150 Ma. Age peaks identified in the PDD analysis are at: 439, 509, 709, 819, 1034 and 1484 Ma.

Supplementary Paper 5

**Igneous and metamorphic age spectra of inherited zircon in newly analysed samples**

On subsequent pages in this appendix, we present probability density distributions (PDDs) calculated for each of the new samples. These differ from those presented as figures in the main paper because we have examined each of the inherited zircon cores and classified them according to whether their zoning patterns indicate igneous or metamorphic origins. Th/U ratios are commonly used to distinguish igneous from metamorphic grains (*e.g.* Kohn & Kelly, 2018). However, in our dataset this parameter displays no correlation at all with the textural criteria that we have applied, so what we present here are PDDs for igneous and metamorphic zircon cores distinguished purely on textural criteria. In SEM cathodoluminescence images (*e.g.* Figure 4 in the main paper, and in Supplementary Paper 3), cores showing concentric oscillatory zoning or sector zoning were deemed to be igneous. Those lacking zoning or showing weak, cloudy, patchy, mottled, wavy or planar zoning were deemed to be metamorphic; see, *e.g.* Wu & Zheng (2004).

To produce the spectra below, we tabulated the ^{206}Pb/^{238}U spot ages for each of the zircon cores with dates > 400 Ma, representing the average rock crystallisation age of *ca* 370 Ma (Clemens *et al.*, 2022) of the rocks plus a 30 Myr margin. As in the main paper, these zircon cores were then considered certainly inherited. Spot ages were rounded up to the nearest 1 Ma and then processed, with a notional 1σ bandwidth of 30 Ma (*e.g.* Andersen *et al.*, 2017) and a 5 Ma bin size, to produce PDDs. Only spot ages with 90 to 110% concordance were used. In the PDDs below, we have overlain the metamorphic spectra (in orange) on the igneous spectra (in blue) so that any correlations and contrasts can be clearly seen.

The spectra appear somewhat different from those presented in the main paper because of the separate processing of the igneous and metamorphic cores. As in the main paper, the spectra are organised according to the tectonometamorphic zone in which their host rocks occur, and then grouped according to whether the rock is S- or I-type (*e.g.* Chappell & White, 2001). The spectra are analysed below, but discussion of their significance can be found in the main text of the paper.

Granitic rocks of the Stawell and Bendigo zones

*Late Devonian I-type Mount Bute Granite (monzogranite) – MB1*
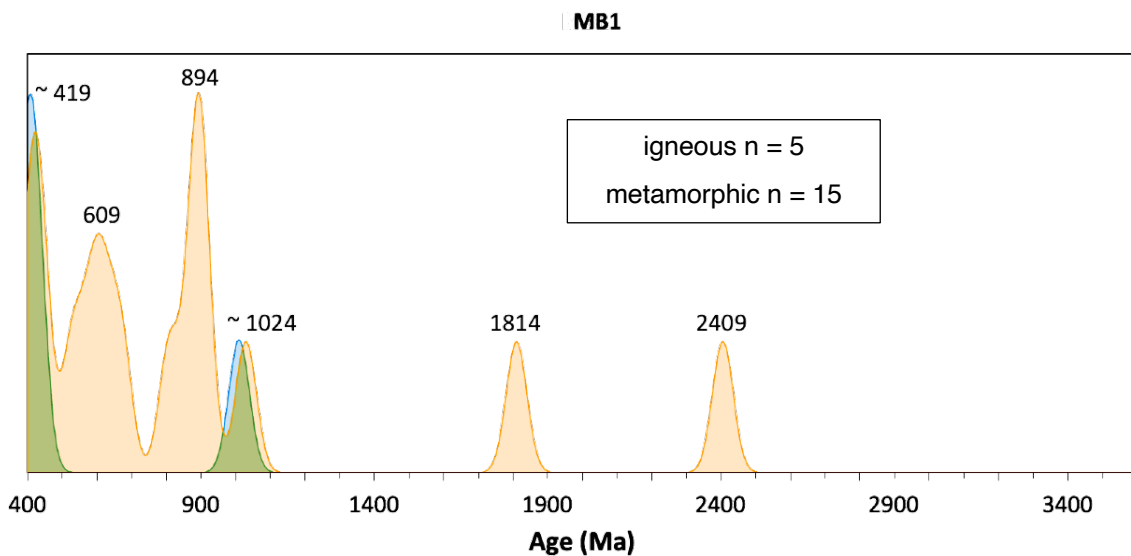
For both igneous and metamorphic cores, this sample has a prominent earliest Devonian peak at *ca* 419 Ma. The rest of the inheritance is Proterozoic, and dominated by zircon grains that record metamorphic events, with a shared igneous and metamorphic peak at *ca* 1024 Ma.

Late Devonian I-type Ercildoun Granite (porphyritic monzogranite variety) – AD1
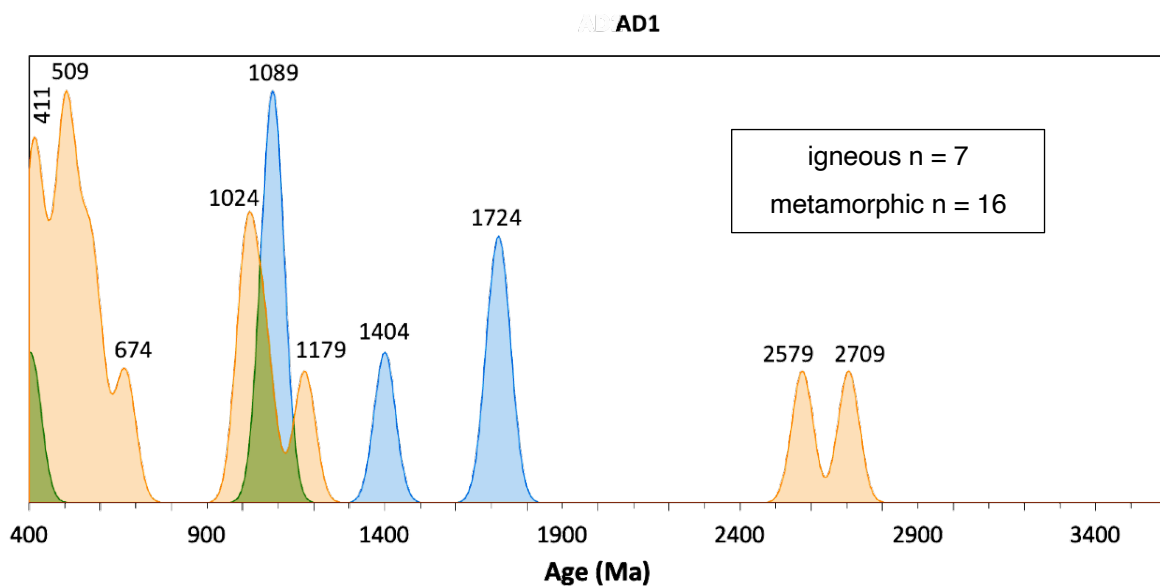

In this rock, both spectra have an earliest Devonian peak at 411 Ma. The rest of the igneous peaks lie between 1089 and 1724, with a discernible spike at 1404 Ma. The metamorphic peaks form 3 groups — mid-Cambrian to late Neoproterozoic 509 to 674 Ma, late Mesoproterozoic 1024 to 1179 Ma and Neoarchean peaks at 2579 and 2709 Ma.

Late Devonian Mount Alexander pluton, S-type variety – HAR17

HAR17
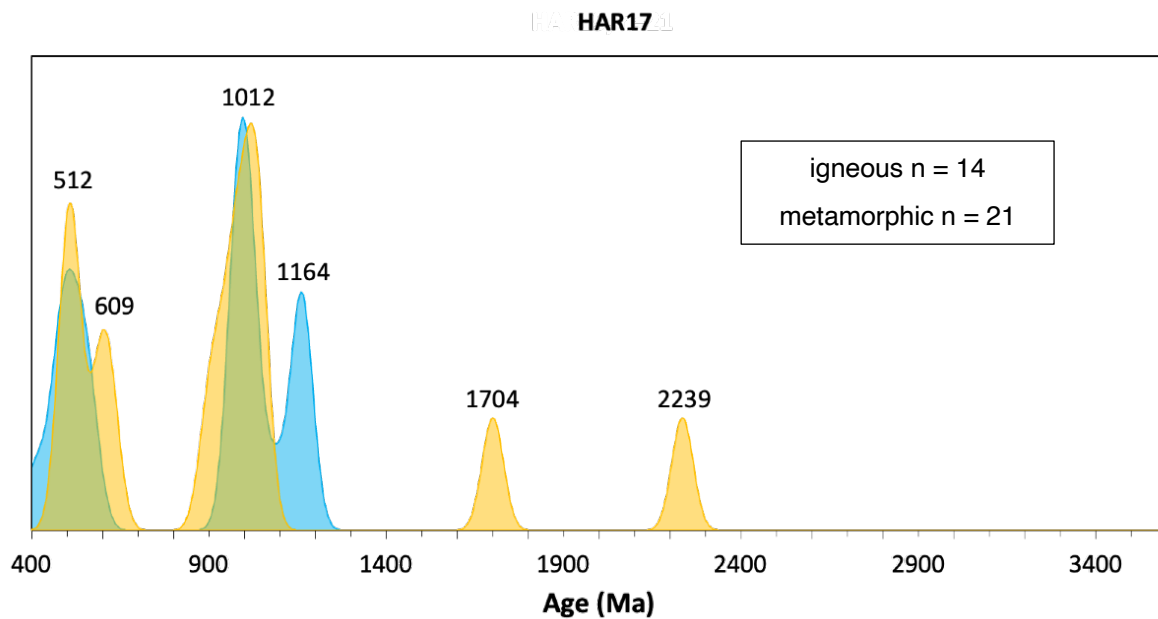
Unlike the previous two rocks in these zones, this S-type unit of the Mount Alexander pluton, in the Harcourt batholith, contains no Early Devonian inheritance, but igneous and metamorphic age peaks coincide, recording events at 512 and 1012 Ma. There are definite similarities with the spectrum for the Ercildoun I-type granite, in the pre-1400 Ma section, but there is no 1400 Ma peak, and the older metamorphic events (1704 and 2239 Ma) are peculiar to this sample.

*Late Devonian Baringhup pluton, I-type variety – HAR19*

HAR19
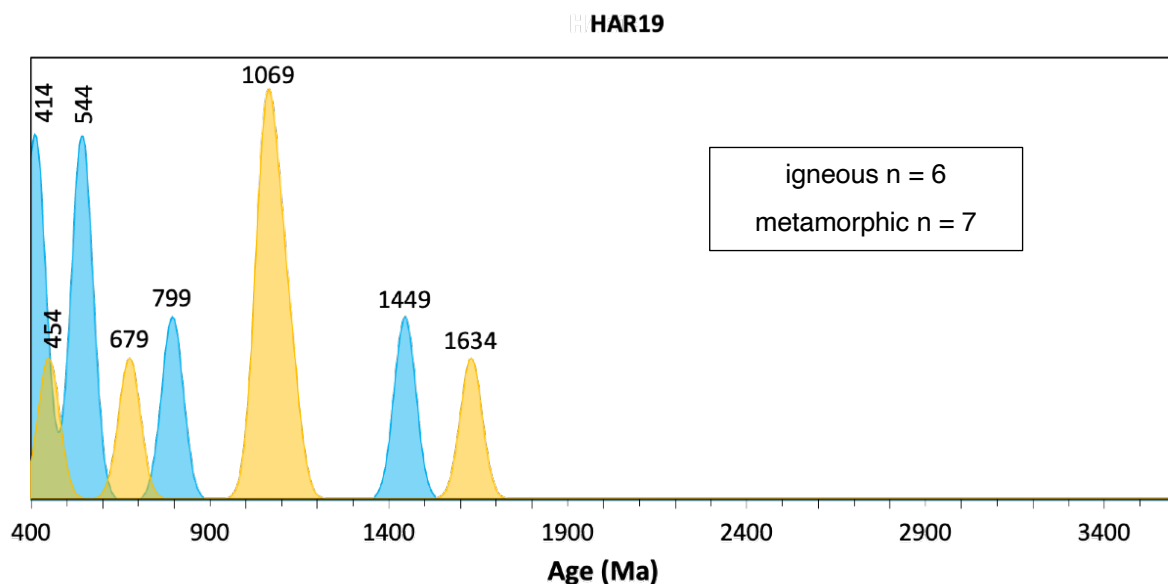
In contrast with its neighbouring S-type sample (HAR17), this I-type rock, from the Baringhup pluton, does contain igneous zircon with a prominent earliest Devonian age peak at 414 Ma, also recording igneous events at 544, 799 and 1449 Ma. The metamorphic spectrum is dominated by zircon that documents an event at 1069 Ma, with other events at 454, 679 and 1634 Ma. The igneous peak at 1449 Ma and the metamorphic peak at 1634 Ma may jointly constitute a Selwyn Block signature; granitic and metamorphic rocks of *ca* 1600 Ma age are inferred to form the unexposed basement in Tasmania; see the main text for details. In contrast to the other samples from these zones, this rock contains no older Mesoproterozoic or Archean inheritance.

Late Devonian granitic rocks of the Melbourne Zone

S-type monzogranite from the Mount Wombat pluton, Strathbogie batholith – S1
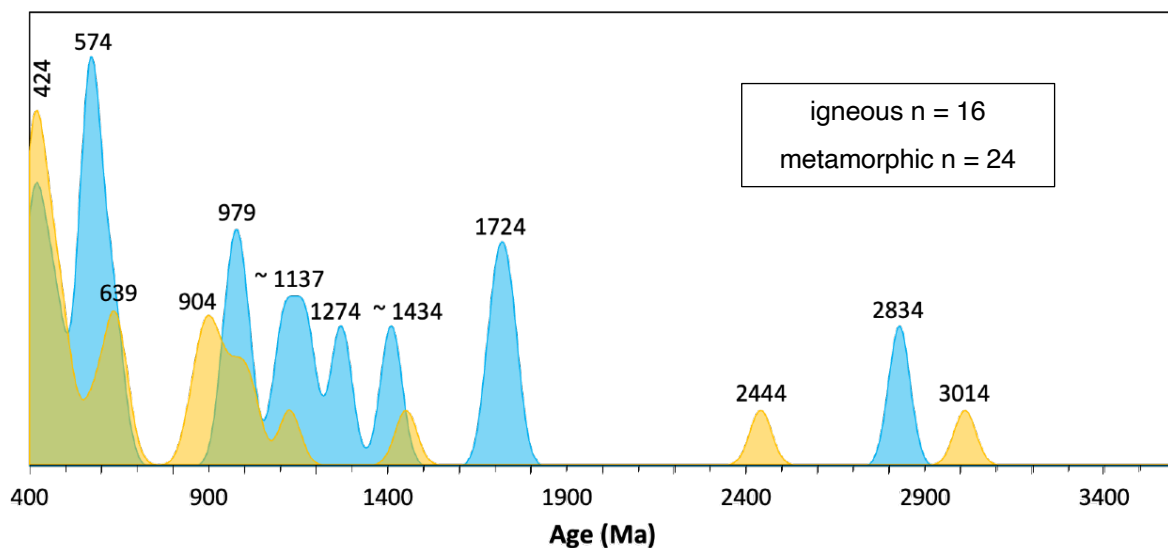
Both the igneous and metamorphic spectra for the zircon in this rock are complex, with numerous age peaks. Like many rocks in this dataset, there are young and coinciding igneous and metamorphic peaks, but here they are latest Silurian in age (424 Ma). There are general similarities with some rocks in the Stawell and Bendigo zones, with prominent late Neoproterozoic peaks and groups in the early Neoproterozoic to Mesoproterozoic, including both igneous and metamorphic peaks at around 1434 Ma, a possible Selwyn Block signature. Prominent igneous evens are recorded at 574 and 1724 Ma, and there are early igneous and metamorphic events reflected in peaks at 2444 to 3014 Ma.

S-type granodiorites from the Mount Disappointment nested laccolith – MD27 and MD50

Both these samples are S-type, but MD50 is more strongly so, having redder-coloured (higher-Al and -Ti) biotite, slightly higher ASI (mol. $Al_2O_3/[CaO-3.33P_2O_5+Na_2O+K_2O]$) and higher K_2O/Na_2O. To facilitate comparison, the zircon age spectra are shown together on the following page.
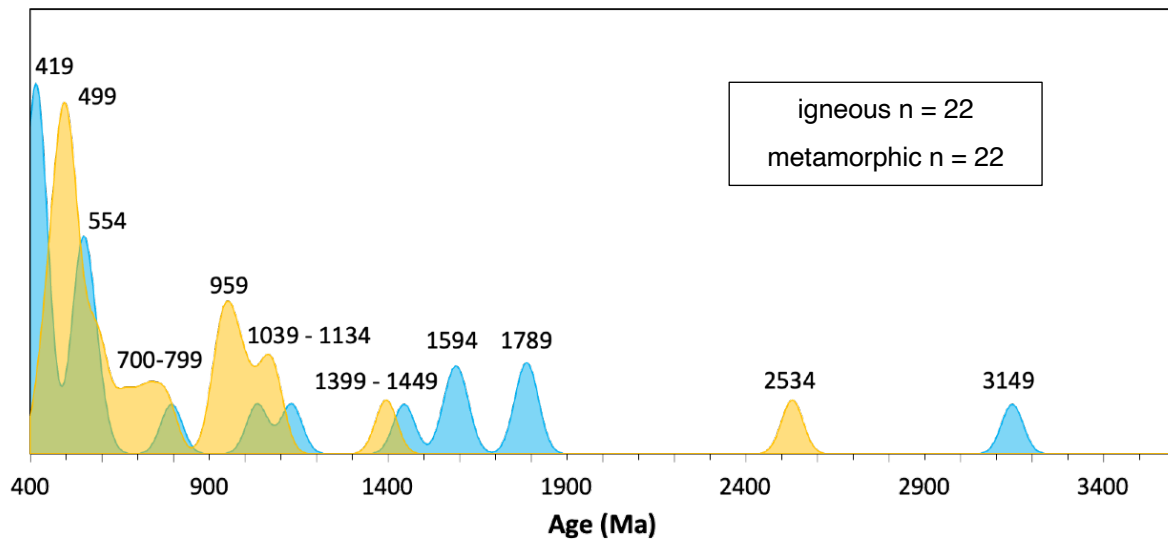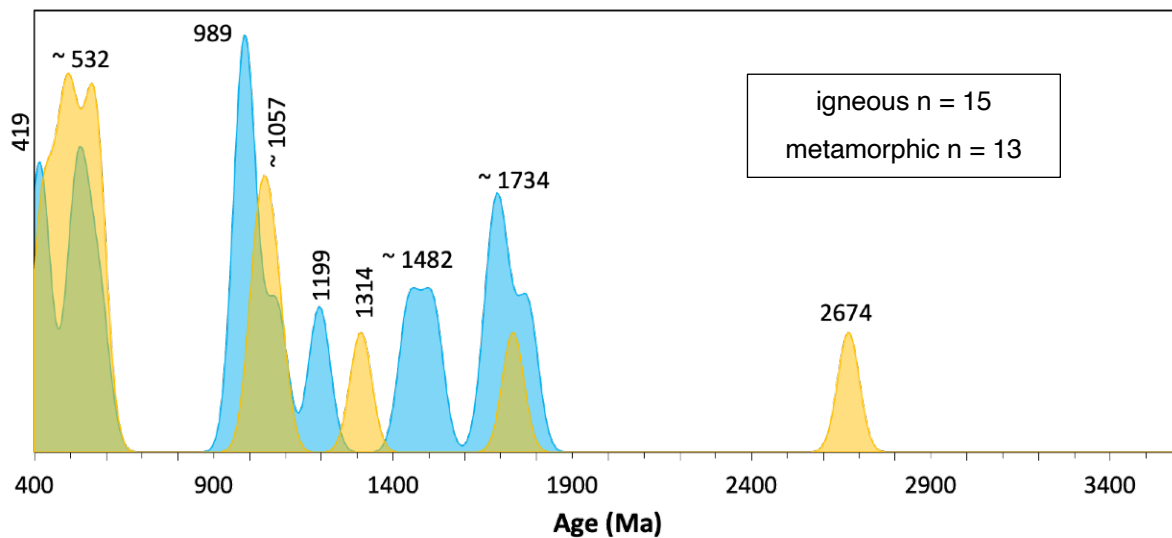
In common with many other rocks in this study, these granodiorites from the Mount Disappointment pluton have earliest Devonian igneous zircon age peaks at 419 Ma, and also record igneous and metamorphic events at around 550 to 500 Ma in the Cambrian and latest Neoproterozoic. However, the similarities more-or-less end there. Leaving aside the few Archean zircon cores in both rocks, MD50 records major igneous events at 989, *ca* 1057, 1199, 1482 and *ca* 1734, all of which are either absent in MD27 or have very weak signals. Beyond the Cambrian, the metamorphic signals also differ very significantly, with major events at 1314 and *ca* 1750 Ma, which are not recorded in the inheritance in MD27. The magma sources clearly differed significantly in their lithological and age structure, which can also be said of the two closely-spaced samples from the Baringhup pluton. It thus seems that source variations are common, quite significant in magnitude, and also vary on small spatial scales.

I-type Lysterfield Granodiorite – L1

L1
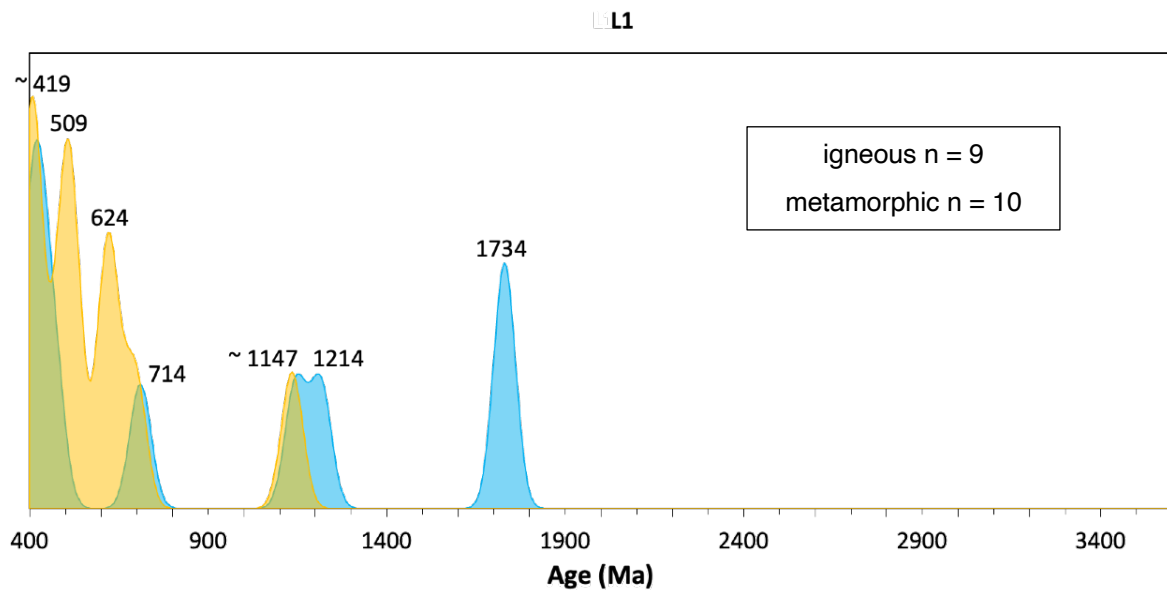
Like many of the rocks studied here, this strongly I-type hornblende biotite granodiorite also carries zircon that attests to both igneous and metamorphic events in the earliest Devonian (*ca* 419 Ma). The common metamorphic events around 500 and 620 Ma are also present. There appear to be few similarities in the pattern of peaks to the rocks from nearby Mount Disappointment, except for the prominent igneous event at *ca* 1734 Ma, which also appears in MD50 and S1, in the Melbourne Zone, and AD1 in the Stawell Zone.

Monzogranite from the Tynong pluton of the Tynong batholith – TY2

TY2
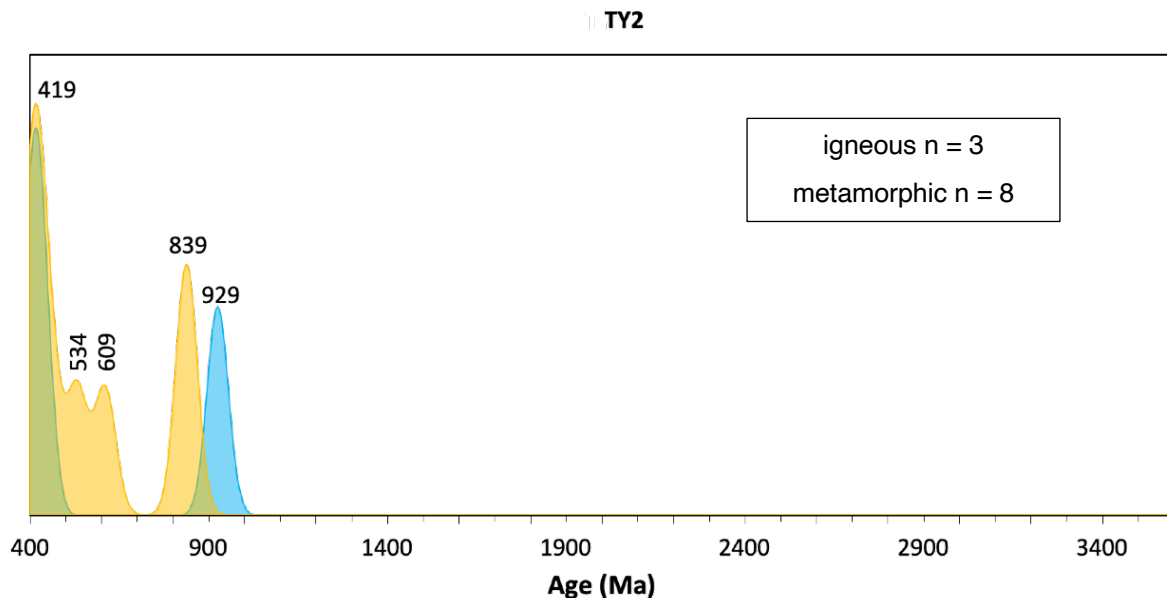
Like the Lysterfield Granodiorite, the Tynong pluton is also a hornblende-bearing, strongly I-type unit. However, no other non-A-type sample in the present set rivals TY2 for the simplicity of its inherited-zircon age spectrum. Again, as with many of the rocks studied here, there are prominent, shared peaks for an igneous and metamorphic event at 419 Ma, in the earliest Devonian, but the only other igneous peak lies at 929 Ma, which has no counterpart in any other spectrum determined here. The usual metamorphic peaks in the range of 500 to 600 Ma are present, but the peak at 839 is not reflected in any other spectrum, apart from sample MB1, from the Stawell Zone. No inheritance older than the Neoproterozoic is recorded in this rock.

Early Devonian granitic rock from the Bassian Tasement Terrane

Mafic schliere from the S-type Oberon pluton, Wilsons Promontory batholith – WPB7
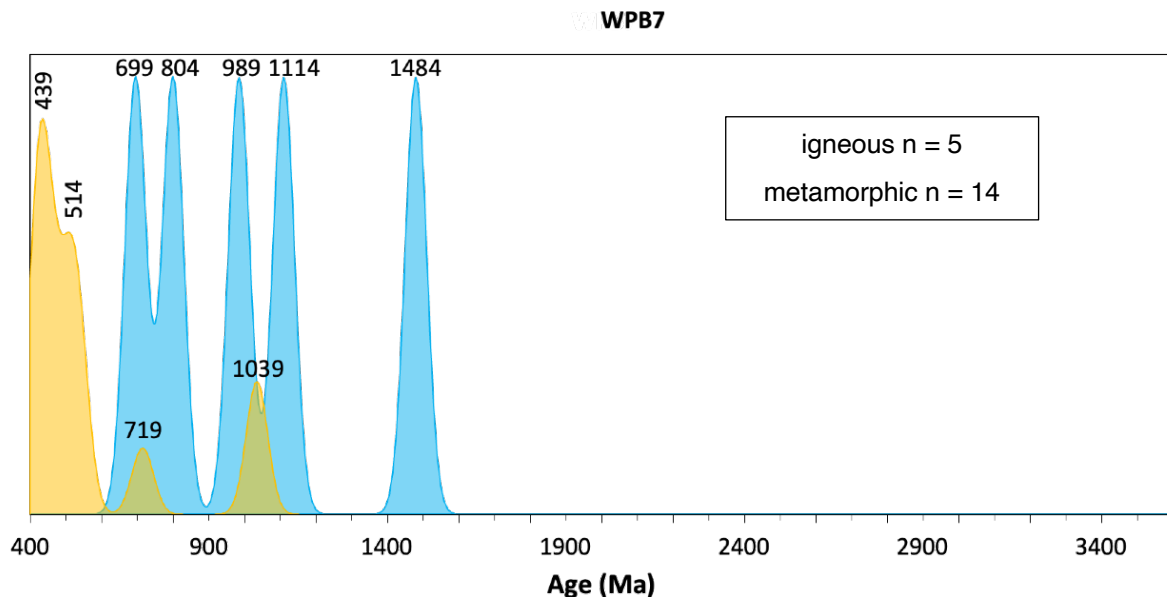
Inherited zircon in this Early Devonian pluton records an early Silurian metamorphic event at 439 Ma, along with the more common (*ca* 510 Ma) middle Cambrian metamorphic event. This is followed by peaks at 719 and 1039 Ma, which are both common in Melbourne Zone granitic rocks. The igneous zircon cores attest to magmatic events at 699, 804, 989, 114 and 1484 Ma. The last of these may be a Selwyn Bock event, but is somewhat earlier than expected.

References

Andersen, T., Kristoffersen, M., & Elburg, M. A. (2017). Visualizing, interpreting and comparing detrital zircon age and Hf isotope data in basin analysis – a graphical approach. *Basin Research*, *30*(1), 132–147. https://doi.org/https://doi.org/10.1111/bre.12245

Chappell, B. W., & White, A. J. R. (2001). Two contrasting granite types: 25 years later. *Australian Journal of Earth Sciences*, *48*(4), 489–499. https://doi.org/10.1046/j.1440-0952.2001.00882.x

Clemens, J. D., Stevens, G., & Coetzer, L. M. (2022). Dating initial crystallisation of some Devonian plutons in central Victoria, and geological implications. *Australian Journal of Earth Sciences*, in press.

Kohn, M. J., & Kelly, N. M. (2018). Petrology and geochronology of metamorphic zircon. In D. E. Moser, F. Corfu, J. R. Darling, S. M. Reddy, & K. Tait (Eds.), *Microstructural Geochronology: Planetary Records Down to Atom Scale*. American Geophysical Union. https://doi.org/10.1002/9781119227250.ch2

Wu, Y., & Zheng, Y. (2004). Genesis of zircon and its constraints on interpretation of U–Pb age. *Chinese Science Bulletin*, *49*(15), 1554–1569. https://doi.org/10.1007/BF03184122